Open Research Online

The Open University's repository of research publications
and other research outputs

The lunar Dhofar 1436 meteorite: ^{40}Ar ^{39}Ar chronology and volatiles, revealed by stepwise combustion and crushing methods

Journal Item

How to cite:

Korochantseva, Ekaterina V.; Buikin, Alexei I.; Hopp, Jens; Verchovsky, Alexander B.; Korochantsev, Alexander V.; Anand, Mahesh and Trieloff, Mario (2021). The lunar Dhofar 1436 meteorite: 40Ar 39Ar chronology and volatiles, revealed by stepwise combustion and crushing methods. Meteoritics & Planetary Science (Early Access).

For guidance on citations see FAQs.

© 2021 The Authors

https://creativecommons.org/licenses/by/4.0/

Version: Version of Record

Link(s) to article on publisher's website:
http://dx.doi.org/doi:10.1111/maps.13632

Copyright and Moral Rights for the articles on this site are retained by the individual authors and/or other copyright owners. For more information on Open Research Online's data policy on reuse of materials please consult the policies page.

oro.open.ac.uk

Check for updates

The Meteoritical Society

Meteoritics & Planetary Science 1–27 (2021)
doi: 10.1111/maps.13632

The lunar Dhofar 1436 meteorite: ^{40}Ar-^{39}Ar chronology and volatiles, revealed by stepwise combustion and crushing methods

Ekaterina V. KOROCHANTSEVA[1,2], Alexei I. BUIKIN[2], Jens HOPP[1], Alexander B. VERCHOVSKY[3], Alexander V. KOROCHANTSEV[2], Mahesh ANAND[3,4], and Mario TRIELOFF[1]*

[1]Institut für Geowissenschaften, Klaus-Tschira-Labor für Kosmochemie, Universität Heidelberg, Im Neuenheimer Feld 234-236, 69120 Heidelberg, Germany
[2]Vernadsky Institute of Geochemistry, Kosygin St. 19, 119991 Moscow, Russia
[3]School of Physical Sciences, The Open University, Milton Keynes MK7 6AA, UK
[4]Department of Earth Sciences, The Natural History Museum, London SW7 5BD, UK
*Corresponding author. E-mail: mario.trieloff@geow.uni-heidelberg.de

(Received 13 September 2018; revision accepted 09 January 2021)

Abstract–The lunar meteorite Dhofar 1436 is dominated by solar wind type noble gases. Solar argon is equilibrated with "parentless" ^{40}Ar commonly known as lunar orphan argon. Ar-Ar isochron analyses determined the lunar trapped ^{40}Ar/^{36}Ar ratio to 2.51 ± 0.04, yielding a corrected plateau age of 4.1 ± 0.1 Ga, consistent with the lunar Late Heavy Bombardment period. Lunar trapped and radiogenic argon components are all released at high temperatures (1200–1400 °C). Surprisingly, solar noble gases and lunar trapped argon can largely be released by crushing. Initial crushing steps mainly release elementally fractionated solar wind gases, while in advanced crushing steps, cosmogenic components dominate. Cosmogenic noble gases indicate irradiation at the lunar surface; they are less fractionated than solar wind species. We favor a scenario in which both solar and a large fraction of cosmogenic gases were acquired before the 4.1 Ga event, which caused shock metamorphism and formation of the regolith breccia. Sintering and agglutination along grain boundaries resulted in mobilization of solar wind, reimplanted, radiogenic, and cosmogenic noble gases, and resulted in their partial homogenization, fractionation, and retrapping in voids and/or defects accessible by crushing. An alternative scenario would be complete reset of the K-Ar system 4.1 Ga ago accompanied by loss of all previously accumulated solar and cosmogenic noble gases. Later, the precursor of Dhofar 1436 became lunar regolith and accumulated solar and cosmogenic noble gases and reimplanted ^{40}Ar before its final formation of the polymict impact breccia. The C abundance of the step-combusted Dhofar 1436 is 555.3 ppm, with δ^{13}C of −28‰ to +11‰. Nitrogen contents released by crushing and combustion are 3.2 ppm and 20.8 ppm, respectively. The lightest nitrogen composition (δ^{15}N = −79‰) is likely due to release from voids of shock metamorphic phases and is rather a result of the mobilization of nitrogen components that accumulated prior to the 4.1 Ga event.

INTRODUCTION

Lunar meteorites provide important information complementing studies of the Apollo and Luna samples and also complementing orbital and regional remote sensing observations of the Moon. They potentially provide a more diverse sampling of the lunar surface than the returned lunar rocks from the Apollo and Luna missions, which were restricted to the equatorial and nearside landing sites. Here, we report the results of a high-resolution ^{40}Ar-^{39}Ar stepwise heating study and noble gas, nitrogen, carbon stepwise combustion, and crushing analyses of the lunar feldspathic impact melt breccia Dhofar 1436 (Connolly et al. 2008).

© 2021 The Authors. Meteoritics & Planetary Science published by Wiley Periodicals LLC on behalf of The Meteoritical Society (MET).
This is an open access article under the terms of the Creative Commons Attribution-NonCommercial-NoDerivs License, which permits use and distribution in any medium, provided the original work is properly cited, the use is non-commercial and no modifications or adaptations are made.

^{40}Ar-^{39}Ar dating has been used extensively in previous studies to decipher the lunar chronology, to develop the late heavy bombardment (LHB) hypothesis (e.g., Tera et al. 1974; Turner 1977), and to highlight the topic of the lunar trapped argon (e.g., see Eugster et al. 2001). While laser-assisted ^{40}Ar-^{39}Ar dating yields isotopic data on small spatial scales (e.g., Cohen et al. 2002, 2005a; Fernandes et al. 2004; Sokol et al. 2008), the high-resolution stepwise heating ^{40}Ar-^{39}Ar analysis of bulk samples is a valuable tool to deconvolve different Ar components on account of their diffusional properties, particularly to separate in situ radiogenic ^{40}Ar from multiple trapped ^{40}Ar components, which otherwise occludes the chronologic information. In lunar samples, indigenous trapped Ar components generally consist of solar wind, fractionated solar wind, planetary (P1 or Q), and orphan Ar (see below). Lunar meteorites found in terrestrial deserts are frequently contaminated by atmospheric argon, which is released during the gas extractions mostly at low and intermediate temperature steps (<1000 °C; e.g., Korochantseva et al. 2016). Such atmospheric Ar can be well separated from the indigenous high-temperature lunar trapped components (Fernandes et al. 2000; Korochantseva et al. 2016). In addition, the isochron analysis, used in the high-resolution ^{40}Ar-^{39}Ar dating for deconvolution of radiogenic and trapped Ar components, is a suitable method for precise evaluation of the extraterrestrial trapped argon composition (Korochantseva et al. 2007). Another advantage of this high-resolution technique is that a complicated irradiation history—lunar meteorites typically experienced irradiation in different geometries and for different durations—can be distinguished in favorable cases by using the ^{37}Ar-$^{38}Ar_{cos}$ cosmic-ray exposure (CRE) age spectrum (Korochantseva et al. 2016).

The so-called lunar "orphan" argon is believed to be a time-dependent component in lunar rocks (Yaniv and Heymann 1972; Heymann et al. 1974; Eugster et al. 2001; Wieler and Heber 2003) and it is used to estimate the time that has elapsed since the solar wind had been acquired (Joy et al. 2011; Fagan et al. 2014). This antiquity model considers lunar trapped Ar as a mixture of solar wind Ar and radiogenic ^{40}Ar degassed from the lunar interior and being reimplanted by the actions of solar wind into lunar surface rocks. Ozima et al. (2004) noted quantitative problems with the origin of the orphan argon according to the "antiquity" scenario. There are data (Fernandes et al. 2000, 2003; Cohen et al. 2005b; Korochantseva et al. 2016) inconsistent with the empirical antiquity model (Eugster et al. 2001), raising the issue about a simple relation between age and the trapped $^{40}Ar/^{36}Ar$ ratio in lunar samples.

The isotopic composition of N in lunar soils is also considered as an antiquity measure (Becker and Clayton 1975) and its apparent variation over time has been initially interpreted in terms of secular evolution of the nitrogen isotopic composition of the solar wind from lower to higher $^{15}N/^{14}N$ ratios (Kerridge 1975, 1989; Becker and Clayton 1975). However, Geiss and Bochsler (1982) challenged this hypothesis and proposed a constant nitrogen isotope composition in the solar wind during the last 4 Ga. Later, it was demonstrated that the nitrogen isotope composition in the solar corpuscular radiation has not changed significantly over time (Owen et al. 2001; Meshik et al. 2007; Marty et al. 2010, 2011). Alternatively, the significant fluctuations in the trapped $\delta^{15}N$ values of up to 300‰ observed in lunar regolith of the Apollo 17 and Luna 24 missions were interpreted by variable mixing between the isotopically light solar nitrogen and isotopically heavy nitrogen of planetary origin continuously accreting to the Moon (Hashizume et al. 2002; Füri et al. 2012; Mortimer et al. 2016). Based on the regolith analyses of presumably recently exposed Luna 24 and Apollo samples, Füri et al. (2012) argued that the variations are not due to different sampling locations. The increase in $\delta^{15}N$ with decreasing antiquity was related by Hashizume et al. (2002) to the recently increased micrometeorite flux to the lunar surface during the last 0.5 Ga, that is, due to variations in time, rather than in space. Indeed, the Genesis mission data proved that nitrogen in lunar regolith is dominated by non-solar sources (Mortimer et al. 2016; Wieler 2016). However, the antiquity nitrogen model still requires an explanation and not only for the last 0.5 Ga (Hashizume et al. 2002).

Our preliminary ^{40}Ar-^{39}Ar analyses showed that Dhofar 1436 is a gas-rich meteorite containing significant concentrations of solar and lunar trapped noble gases. As a next step, we conducted a combined noble gas, nitrogen, and carbon stepwise crushing and combustion study to constrain the siting and origin of lunar trapped argon and its relation to the composition of trapped nitrogen, carbon, and other noble gas components.

While the stepwise heating gas extraction technique is well established since the 1970s in cosmochemistry (e.g., Friedman et al. 1970; Hohenberg et al. 1970; Turner 1970), stepwise vacuum crushing is largely used for investigations of terrestrial mantle samples to extract gases from inclusions avoiding interferences with gases located in the crystal lattice. It allows separation of gases of genetically distinct inclusions, which could be formed during primary and secondary events, by gradual opening of voids/inclusions of different sizes (e.g., Buikin et al. 2005, 2014; Hopp et al. 2007). The application of this method to extraterrestrial materials is relatively uncommon mainly

due to the low amounts of released gases. Nevertheless, total or stepwise vacuum crushing has been performed for different classes of meteorites (Martian: Wiens 1988; Ott et al. 1996; Murty and Mahajan 2004; Koike et al. 2017; E-chondrites: Takaoka and Nakamura 1996; Okazaki et al. 2010; ordinary and carbonaceous chondrites: Fukuda et al. 1996; Korochantseva et al. 2018; ureilites: Okazaki et al. 2003; aubrites: Miura et al. 2007; Buikin et al. 2013, 2015; Acapulco-like primitive achondrites: Takaoka et al. 1998) and lunar returned samples not only in the 1970s (e.g., Funkhouser et al. 1971; Heymann and Yaniv 1971; Gibson and Andrawes 1978; Gibson et al. 1979) but also recently (Bekaert et al. 2015, 2018; Verchovsky et al. 2017). In this study, stepwise crushing is applied to a lunar meteorite for the first time.

SAMPLE DESCRIPTION

The lunar feldspathic impact melt breccia Dhofar 1436 (Connolly et al. 2008), consisting of lithic and mineral clasts cemented by a partly devitrified glassy matrix with numerous bubbles, was discovered as a single stone (24.2 g) without fusion crust in the desert of Oman in 2004. According to Connolly et al. (2008), the lithic fragments ranging from 0.01 to 7 mm in size are mainly impact melt breccias and rocks of anorthositic, gabbro-anorthositic, and gabbro-noritic compositions. Granular breccia clasts occur as well. Major minerals are pyroxene (orthopyroxene $En_{68.2–84.1}Wo_{0.2–5.0}$ and clinopyroxene $En_{13.4–63.7}Wo_{12.8–40.5}$) and feldspar ($An_{92.5–98.7}Ab_{1.1–7.2}$), with minor olivine ($Fo_{42.6–72.7}$). Accessory minerals include silica, Al-Ti-chromite, ilmenite, Ca-phosphate, troilite, and FeNi metal (Connolly et al. 2008). This relatively unweathered rock is likely paired with the meteorite Dhofar 1443 (Righter and Gruener 2013).

Two whole rock (WR) samples (Dhofar 1436-a and Dhofar 1436-b) weighing 25.8 and 31.1 mg were used for ^{40}Ar-^{39}Ar dating. Our previous study of the meteorite Dhofar 280 (Korochantseva et al. 2016) has demonstrated that significant chronological and geochemical information could be obtained by analyzing a WR chip of the Dhofar 280 lunar impact melt breccia. The sample Dhofar 1436-b contained a higher proportion of clastic material than Dhofar 1436-a. The bulk contents of Ca (11.9 wt%) and K (0.03 wt%) reported by Connolly et al. (2008) for the average glassy matrix composition are in agreement with the bulk contents of Ca (11.15 and 9.13%) and K (392 and 330 ppm) obtained from the ^{40}Ar-^{39}Ar dating (errors: 5%), indicating (as it is usually considered) that glassy matrix is a good proxy for the bulk composition of lunar meteorites.

WR samples were also taken for noble gas measurements: Dhofar 1436-c and Dhofar 1436-d of 117.5 mg and of 19.78 mg (one piece splits) were used for crushing experiments at the University of Heidelberg and at The Open University, respectively; Dhofar 1436-e of 3.117 mg was used for a stepped combustion experiment at The Open University. The powdered samples (Dhofar 1436-c-p of 2.049 mg and Dhofar 1436-d-p of 4.957 mg, retained after Heidelberg and The Open University crushing, respectively) were also studied by stepped combustion methods at The Open University. The particle size of the powder was predominantly <2–3 μm. Note that the material of powdered samples contains the steel particles from the crusher abrased as a result of friction between the different metal parts. This known problem often results in an overestimation of the sample mass and therefore in an underestimation of the noble gas concentrations.

EXPERIMENTAL TECHNIQUES

Ar-Ar Dating (University of Heidelberg)

^{40}Ar-^{39}Ar analyses (Table 1) of two WR samples of Dhofar 1436 (Dhofar 1436-a and Dhofar 1436-b, weighing 25.8 and 31.1 mg, respectively) have followed standard procedures given by Jessberger et al. (1980) and Trieloff et al. (1994, 1998, 2003). After cleaning with ethanol, the samples were wrapped in high-purity (99.999%) Al-foil and placed into an evacuated quartz ampoule bracketed by the age monitor standard NL 25 hornblende (2.657 ± 0.004 Ga; Schaeffer and Schaeffer 1977; Schwarz and Trieloff 2007). The ampoule was irradiated for 20 days at the GKSS-reactor in Geesthacht, Germany, with Cd-shielding to suppress the thermal and epithermal neutron fluxes, in particular to reduce contributions from the $^{37}Cl(n,\gamma\beta^-)^{38}Ar$ reaction. The J-value was $(1.09 \pm 0.01) \times 10^{-2}$. Correction factors for interfering isotopes were $(^{36}Ar/^{37}Ar)_{Ca} = (4.6 \pm 0.1) \times 10^{-4}$, $(^{38}Ar/^{37}Ar)_{Ca} = (8.8 \pm 0.2) \times 10^{-5}$, $(^{39}Ar/^{37}Ar)_{Ca} = (9.6 \pm 0.1) \times 10^{-4}$, and $(^{38}Ar/^{39}Ar)_K = (7.67 \pm 0.17) \times 10^{-3}$. $(^{40}Ar/^{37}Ar)_{Ca} = (3 \pm 3) \times 10^{-3}$ was determined by Turner (1971) and $(^{40}Ar/^{39}Ar)_K = (1.23 \pm 0.24) \times 10^{-2}$ by Brereton (1970). The samples were stepwise heated from 400 °C to 1380 °C (up to 33 temperature steps) using a resistance-heated furnace with ^{40}Ar blank values of (7–9) × 10^{-10} cm^3 STP at 900 °C and (21–22) × 10^{-10} cm^3 STP at 1380 °C (10 min heating duration). During and after heating, the released gas was in contact with one hot (400 °C) and two cold Zr-Al-getters and one hot Ti-getter. The sample and blank measurements were alternated with analyses of calibration gas having a composition of air ($^{40}Ar/^{36}Ar = 295.5 \pm 0.5$; Steiger and Jäger 1977), which

Table 1. Measured argon isotope data corrected for mass discrimination, sensitivity, system blanks, decay, and relative neutron doses. The instrument sensitivity was 1.6×10^{-9} cm^3 STP/nA. All isotopes are corrected for interfering isotopes produced on K and Ca during irradiation.

Temp. (°C)	$^{36}Ar*10^{-9}$	$^{37}Ar*10^{-10}$	$^{38}Ar*10^{-10}$	$^{39}Ar*10^{-11}$	$^{40}Ar*10^{-8}$	Ar-Ar age	CRE age
a. Dhofar 1436-a (25.8 mg). $(^{40}Ar/^{36}Ar)_{trapped} = 0.0001 \pm 0.0001$							
400	1 ± 1	14 ± 2	3 ± 1	9 ± 1	25 ± 1	6244 ± 216	229 ± 43
450	2 ± 1	43 ± 2	9 ± 1	19 ± 1	49 ± 1	6134 ± 67	287 ± 16
500	6 ± 1	181 ± 5	23 ± 1	64 ± 2	97 ± 2	5176 ± 17	160 ± 4
550	24 ± 1	552 ± 14	65 ± 2	164 ± 4	527 ± 13	6475 ± 17	94 ± 2
580	13 ± 1	494 ± 13	37 ± 1	98 ± 3	252 ± 6	6083 ± 31	62 ± 2
620	17 ± 1	850 ± 22	48 ± 1	122 ± 3	244 ± 6	5645 ± 13	44 ± 1
670	26 ± 1	1310 ± 34	62 ± 2	127 ± 4	263 ± 6	5712 ± 23	26 ± 1
730	24 ± 1	1680 ± 53	54 ± 2	109 ± 4	143 ± 4	4929 ± 23	15 ± 1
800	39 ± 1	1821 ± 56	83 ± 3	131 ± 4	155 ± 5	4755 ± 15	17 ± 1
870	102 ± 3	950 ± 30	207 ± 6	98 ± 3	112 ± 3	4697 ± 16	50 ± 5
940	121 ± 4	811 ± 26	245 ± 8	80 ± 3	90 ± 3	4687 ± 40	70 ± 8
1000	219 ± 7	900 ± 28	436 ± 13	83 ± 3	169 ± 5	5690 ± 31	96 ± 10
1060	423 ± 13	1309 ± 41	838 ± 25	106 ± 3	172 ± 5	5296 ± 19	188 ± 21
1100	870 ± 26	1642 ± 50	1690 ± 50	112 ± 4	280 ± 8	6034 ± 24	230 ± 30
1120	1022 ± 9	930 ± 9	1977 ± 14	59 ± 1	290 ± 2	7211 ± 32	445 ± 63
1140	1888 ± 15	972 ± 9	3582 ± 24	64 ± 2	515 ± 3	8094 ± 44	514 ± 101
1150	1403 ± 12	665 ± 9	2694 ± 19	42 ± 1	384 ± 2	8318 ± 54	739 ± 115
1160	1539 ± 13	830 ± 8	2923 ± 18	50 ± 2	430 ± 2	8224 ± 53	508 ± 120
1170	3585 ± 29	1759 ± 15	6694 ± 38	112 ± 3	978 ± 4	8250 ± 52	305 ± 125
1180	2569 ± 21	1199 ± 10	4809 ± 28	73 ± 1	686 ± 3	8385 ± 29	360 ± 133
1190	3347 ± 27	1894 ± 14	6251 ± 35	115 ± 2	928 ± 4	8100 ± 25	267 ± 108
1200	2855 ± 23	1456 ± 12	5341 ± 31	85 ± 1	775 ± 3	8325 ± 23	321 ± 122
1210	3359 ± 27	1947 ± 15	6274 ± 36	112 ± 1	918 ± 4	8135 ± 22	263 ± 106
1220	4078 ± 33	2407 ± 18	7612 ± 43	133 ± 2	1125 ± 5	8190 ± 24	250 ± 104
1230	3259 ± 26	1906 ± 14	6062 ± 35	110 ± 3	888 ± 4	8114 ± 48	208 ± 105
1240	2056 ± 17	1741 ± 14	3899 ± 24	100 ± 2	594 ± 3	7567 ± 27	311 ± 75
1250	819 ± 7	888 ± 9	1572 ± 12	46 ± 1	246 ± 1	7387 ± 53	324 ± 63
1280	1168 ± 9	1289 ± 9	2220 ± 15	71 ± 1	345 ± 2	7193 ± 26	252 ± 55
1310	993 ± 9	1616 ± 15	1902 ± 14	88 ± 2	313 ± 2	6646 ± 36	204 ± 41
1330	2930 ± 20	2264 ± 16	5392 ± 29	113 ± 1	792 ± 3	7848 ± 20	62 ± 65
1350	5473 ± 35	4242 ± 26	10246 ± 50	200 ± 2	1542 ± 6	8023 ± 19	217 ± 61
1380	1910 ± 15	1898 ± 15	3628 ± 23	91 ± 2	552 ± 3	7596 ± 36	275 ± 59
1380	839 ± 25	896 ± 24	1616 ± 48	28 ± 4	241 ± 5	8214 ± 242	356 ± 228
Total	46982 ± 98	43360 ± 140	88500 ± 150	3013 ± 15	15121 ± 27	7260 ± 9	
b. Dhofar 1436-b (31.1 mg). $(^{40}Ar/^{36}Ar)_{trapped} = 0.0001 \pm 0.0001$							
400	1 ± 1	14 ± 2	5 ± 1	6 ± 1	40 ± 2	7721 ± 309	410 ± 44
500	27 ± 1	1292 ± 36	123 ± 3	356 ± 10	716 ± 19	5658 ± 11	136 ± 1
540	11 ± 1	423 ± 12	37 ± 1	107 ± 3	211 ± 6	5620 ± 22	97 ± 2
580	11 ± 1	398 ± 11	33 ± 1	74 ± 2	143 ± 4	5595 ± 30	78 ± 2
640	15 ± 1	672 ± 19	45 ± 1	99 ± 3	177 ± 5	5450 ± 24	61 ± 1
700	16 ± 1	627 ± 18	44 ± 1	92 ± 3	209 ± 6	5868 ± 23	58 ± 1
750	16 ± 1	550 ± 16	40 ± 1	73 ± 2	97 ± 3	4957 ± 25	46 ± 1
800	17 ± 1	388 ± 7	38 ± 1	50 ± 1	106 ± 2	5763 ± 40	44 ± 2
860	27 ± 1	499 ± 9	59 ± 1	65 ± 2	65 ± 1	4485 ± 28	46 ± 3
940	71 ± 1	698 ± 12	149 ± 3	80 ± 2	74 ± 1	4344 ± 20	64 ± 6
1000	109 ± 2	740 ± 13	222 ± 4	74 ± 2	69 ± 1	4371 ± 29	73 ± 9
1060	207 ± 3	898 ± 15	416 ± 7	82 ± 2	93 ± 1	4695 ± 28	156 ± 17
1100	460 ± 4	995 ± 10	902 ± 8	65 ± 1	155 ± 1	5959 ± 38	236 ± 27
1140	2779 ± 17	1960 ± 13	5229 ± 31	116 ± 2	739 ± 4	7678 ± 28	290 ± 45
1160	5162 ± 32	2303 ± 16	9656 ± 56	136 ± 2	1371 ± 8	8500 ± 27	366 ± 68
1170	2579 ± 16	1551 ± 11	4859 ± 29	81 ± 2	695 ± 4	8207 ± 42	355 ± 54

Table 1. *Continued*. Measured argon isotope data corrected for mass discrimination, sensitivity, system blanks, decay, and relative neutron doses. The instrument sensitivity was 1.6×10^{-9} cm^3 STP/nA. All isotopes are corrected for interfering isotopes produced on K and Ca during irradiation.

Temp. (°C)	^{36}Ar*10^{-9}	^{37}Ar*10^{-10}	^{38}Ar*10^{-10}	^{39}Ar*10^{-11}	^{40}Ar*10^{-8}	Ar-Ar age	CRE age
1180	4167 ± 26	1800 ± 12	7824 ± 45	97 ± 2	1117 ± 6	8738 ± 35	438 ± 71
1190	3098 ± 19	1541 ± 10	5824 ± 34	79 ± 2	837 ± 5	8591 ± 43	400 ± 63
1200	2915 ± 22	1551 ± 12	5490 ± 31	75 ± 2	800 ± 4	8610 ± 52	401 ± 95
1210	2498 ± 19	1507 ± 11	4716 ± 27	72 ± 2	687 ± 3	8398 ± 47	381 ± 85
1225	2621 ± 19	1673 ± 12	4946 ± 29	85 ± 2	725 ± 4	8207 ± 41	354 ± 80
1240	3259 ± 24	2366 ± 16	6148 ± 35	115 ± 3	916 ± 4	8085 ± 37	308 ± 70
1255	2261 ± 17	2159 ± 15	4283 ± 25	97 ± 2	650 ± 3	7771 ± 33	267 ± 54
1275	1292 ± 48	1435 ± 53	2472 ± 91	63 ± 3	382 ± 14	7590 ± 60	294 ± 45
1310	1187 ± 44	1599 ± 59	2270 ± 84	66 ± 3	354 ± 13	7367 ± 58	239 ± 39
1340	1970 ± 73	2990 ± 110	3750 ± 140	120 ± 5	588 ± 21	7225 ± 39	189 ± 31
1350	1385 ± 51	1994 ± 74	2666 ± 99	81 ± 4	417 ± 15	7298 ± 56	259 ± 37
1360	660 ± 26	624 ± 24	1290 ± 49	26 ± 3	197 ± 7	7979 ± 185	515 ± 93
1380	207 ± 10	257 ± 12	411 ± 20	2 ± 2	66 ± 3	10306 ± 2173	476 ± 200
Total	39030 ± 130	35500 ± 170	73940 ± 240	2535 ± 16	12697 ± 43	7257 ± 18	

Remaining argon isotopes are given in cm^3 STP g^{-1} and have the following composition: $^{36}Ar = {}^{36}Ar_{atm} + {}^{36}Ar_{trap} + {}^{36}Ar_{cos}$; $^{37}Ar = {}^{37}Ar_{Ca}$; $^{38}Ar = {}^{38}Ar_{atm} + {}^{38}Ar_{trap} + {}^{38}Ar_{cos} + {}^{38}Ar_{Cl}$; $^{39}Ar = {}^{39}Ar_{K}$; $^{40}Ar = {}^{40}Ar_{rad} + {}^{40}Ar_{atm}$ with atm = terrestrial atmospheric argon; trap = trapped extraterrestrial argon; cos = cosmogenic argon; Ca = argon derived from Ca; Cl = argon derived from Cl; K = argon derived from K; rad = in situ radiogenic argon.

Apparent Ar-Ar ages are calculated using the decay constants given by Steiger and Jäger (1977) and the J-value of $(1.09 \pm 0.01) \times 10^{-2}$. They have been calculated by applying for each temperature extraction a small nominal correction for primordial trapped argon from ^{40}Ar, assuming $^{40}Ar/^{36}Ar = 0.0001 \pm 0.0001$ (Göbel et al. 1978).

CRE (cosmic ray exposure) ages are calculated using the chemical composition of Dhofar 1436 (see the Ar-Ar Dating [University of Heidelberg] section) and the following production rates for $^{38}Ar_{cos}$: (1) for temperature extractions 400–1000 °C—22.09×10^{-10} cm^3/g^{-1}Ma for 4π irradiation (Eugster and Michel 1995); (2) for temperature extraction 1060–1380 °C—13.77×10^{-10} cm^3/g^{-1}Ma for 2π irradiation and a shielding depth of 65 g cm^{-2} (Hohenberg et al. 1978). Solar $(^{36}Ar/^{38}Ar)_{tr}$ ratio is assumed. All ages are given in Ma. The significance of all uncertainties is 1σ.

were used to correct the data for instrumental mass fractionation and to calculate absolute argon concentrations using the peak height method.

The Steiger and Jäger (1977) convention on geochronology is still the most recent convention, including total and partial decay constants of ^{40}K, as well as potassium and argon isotopic compositions, and we consider it inappropriate to replace individual values until a new general consensus is reached based on recent suggestions (Renne et al. 2010, 2011; Schwarz et al. 2011). We particularly emphasize that usage of an alternative argon isotopic composition (e.g., Lee et al. 2006) for air—commonly used a calibration for mass discrimination—will not change our age results. As the age equation in Ar-Ar dating only depends on the ratio $(^{40}Ar/^{39}Ar)_{sample}/(^{40}Ar/^{39}Ar)_{age\ monitor}$, possibly erroneously calculated mass discrimination factors affect both sample and age monitor $^{40}Ar/^{39}Ar$ ratios to the same extent, and will cancel out completely. The uncertainties are reported at 1σ level.

The concentrations of $^{36}Ar_{trapped}$ and $^{38}Ar_{cos}$ in the samples were calculated by component deconvolution using $(^{36}Ar/^{38}Ar)_{cos} = 0.65$ (Eugster et al. 1991) and $(^{36}Ar/^{38}Ar)_{trapped}$ ratios that may vary between planetary (5.35) and solar (5.47) compositions (Heber et al. 2009; see also Raquin and Moreira 2009). While the exact choice of the trapped $^{36}Ar/^{38}Ar$ ratio is not important for Ar-Ar plateau age calculations, it has some influence on the cosmogenic argon content. The CRE ages were calculated using cosmogenic ^{38}Ar and Ca-derived ^{37}Ar concentrations measured for individual extraction steps. The average glassy matrix composition, commonly regarded as the bulk composition of lunar meteorites, was used to calculate the relative contributions of target elements participating in the production of cosmogenic ^{38}Ar: SiO_2 45.1, TiO_2 0.26, Al_2O_3 30.8, FeO 4.49, MgO 3.94, CaO 16.7, Na_2O 0.48, K_2O 0.04 (wt%; Connolly et al. 2008). We applied the model calculations for 2π production by Hohenberg et al. (1978) and for 4π production by Eugster and Michel (1995). For Dhofar 1436, application of the 2π production rate model by Hohenberg et al. (1978) showed that 99.2% of cosmogenic ^{38}Ar is produced from Ca; for a 4π irradiation, the systematics of Eugster and Michel (1995) resulted in an ^{38}Ar contribution of 97.7% from Ca. For more detailed information on the choice of the model calculations and the reliability of the CRE age spectrum, see Korochantseva et al. (2016).

Table 2. He, Ne, and Ar isotope compositions released by crushing in Heidelberg from Dhofar 1436-c (117.5 mg).

Extractions[a]	^{4}He (10^{-8})[b]	^{4}He/^{3}He	^{20}Ne (10^{-8})[b]	^{20}Ne/^{22}Ne	^{21}Ne/^{22}Ne	^{36}Ar(10^{-8})[b]	^{40}Ar/^{36}Ar	^{36}Ar/^{38}Ar	^{4}He/^{20}Ne	^{20}Ne/^{36}Ar
50	1188.1 (38.3)	2158.44 (126.97)	1055.8 (3.9)	12.57 (4)	0.0440 (4)	149.5 (6.3)	7.66 (7)	n.a.	1.13 (4)	7.06 (30)
60	55.2 (1.4)	2258.87 (133.60)	76.5 (3)	12.39 (2)	0.0444 (4)	19.3 (5)	2.88 (4)	5.44 (8)	0.72 (2)	3.97 (10)
120	157.9 (4.0)	1850.08 (108.95)	215.6 (8)	12.26 (4)	0.0450 (5)	65.8 (1.5)	2.77 (3)	5.42 (13)	0.73 (2)	3.27 (8)
200	78.8 (2.0)	2398.95 (141.73)	119.3 (4)	12.42 (2)	0.0442 (3)	44.2 (1.0)	2.34 (2)	5.38 (13)	0.66 (2)	2.70 (6)
400	349.2 (8.8)	1812.68 (106.81)	105.6 (4)	12.24 (3)	0.0455 (4)	142.9 (3.3)	2.11 (2)	5.42 (7)	3.31 (8)	0.74 (2)
700	424.7 (10.7)	1764.37 (103.86)	64.7 (2)	12.11 (4)	0.0476 (7)	132.9 (3.0)	1.95 (2)	5.40 (9)	6.56 (17)	0.49 (1)
1200	427.2 (10.8)	1522.68 (89.62)	168.7 (6)	12.08 (2)	0.0501 (5)	279.6 (6.4)	1.91 (2)	5.28 (7)	2.53 (6)	0.60 (1)
2000	335.4 (8.5)	1546.16 (91.07)	66.8 (2)	11.81 (2)	0.0547 (5)	184.4 (4.2)	1.94 (2)	5.45 (7)	5.02 (13)	0.36 (1)
3000	230.9 (5.8)	1505.62 (88.72)	31.7 (1)	11.53 (2)	0.0620 (5)	78.2 (1.8)	1.99 (2)	5.42 (7)	7.29 (19)	0.41 (1)
4000	71.2 (1.8)	1488.12 (88.03)	9.20 (3)	11.36 (3)	0.0661 (6)	23.9 (6)	2.31 (12)	5.36 (7)	7.73 (20)	0.38 (1)
5000	70.0 (1.8)	1997.81 (118.13)	7.12 (3)	11.24 (4)	0.0646 (7)	19.4 (4)	2.22 (11)	5.30 (7)	9.83 (25)	0.37 (1)
Total	3388.6 (43.7)	1821.68 (49.08)	1921.3 (4.1)	12.16 (1)	0.0489 (1)	1140.1 (11.2)	2.80 (3)	5.38 (8)	1.76 (2)	1.69 (2)

Numbers in parentheses refer to the last digits and are 1σ-uncertainties.
n.a. = not analyzed.
[a]Cumulative number of strokes.
[b]cm^3 STP g^{-1}.

Crushing Experiment for Noble Gas Measurements (University of Heidelberg)

The noble gas analysis of the WR sample (Dhofar 1436-c, weighing 117.5 mg) was performed with an in-house modified VG 3600 mass spectrometer. The sample gas was released by stepwise crushing in a manual ball mill. Hot and cold Ti-sponge and Zr–Al getters were used for gas purification. Ar was trapped on activated charcoal cooled with liquid nitrogen and was thus separated from He and Ne. The latter were trapped on a cryostatically cooled charcoal trap held at 20 K. Subsequently, separation of He and Ne was achieved at 48 K, and, after analysis of He, Ne was released at 120 K to minimize any residual Ar contributions. The mass spectrometer background was monitored before introduction of the sample gases. The ion currents of ^{4}He, ^{40}Ar, and ^{36}Ar were measured directly with a Faraday cup. Helium-3, neon isotopes (masses 20, 21, and 22), and ^{36}Ar were analyzed using an electron multiplier working in ion counting mode. The signal ratio between Faraday cup and electron multiplier was determined regularly (for He before each measurement, for Ar once per month). In the case of Ne, we also routinely detected masses 18, 40, 42, and 44 to correct for mass interferences on neon isotopes. However, these corrections never exceeded 0.1%. The calibration of the mass spectrometer sensitivity and mass discrimination was performed by regular measurements of standard gases having the isotopic composition of air (for Ne, Ar) and with He having a ^{4}He/^{3}He ratio of 40183 ± 87. The system blanks were at the level of instrumental background ($<1 \times 10^{-9}$ cm^3 STP) for ^{4}He (Faraday detector); 5.56×10^{-12} cm^3 STP for ^{20}Ne; 4.02×10^{-12} cm^3 STP for ^{36}Ar. Within experimental uncertainties, the measured blanks were indistinguishable from atmospheric isotopic compositions. The uncertainties given in Table 2 include uncertainties of the standard measurements and interference/blank corrections (blank uncertainty is 20%). The uncertainties of the absolute concentrations of the standard gases are 10%; however, Ne/Ar elemental ratios in standards with air composition are estimated to have an uncertainty of about 5% (mainly due to volume corrections).

^{4}He, Ne, Ar, N, and C Measurements by Stepped Crushing and Combustion Methods (the Open University, UK)

The high-sensitivity Finesse mass spectrometer system at The Open University (Verchovsky et al. 1997) was used for analyses of Dhofar 1436. The WR sample (Dhofar 1436-d) of 19.78 mg was stepwise crushed with 12,100 cumulative strokes. The powdered samples (Dhofar 1436-c-p of 2.049 mg and Dhofar 1436-d-p of 4.957 mg, retained after Heidelberg and The Open University crushing, respectively), and the WR sample (Dhofar 1436-e) of 3.117 mg wrapped in clean platinum foil were combusted in oxygen (pO_2 ~ 5mbar), supplied from CuO, in a double-walled quartz–ceramic furnace. The samples were stepwise heated from 200 °C to 1460 °C (13–15 steps) for 30 min at each temperature step, followed by 15 min for oxygen resorption, before transfer of the produced gases to the cleanup section. Helium-4 and neon (on a quadrupole mass spectrometer) and N_2 and Ar (on a magnetic sector mass spectrometer) were measured for each crushing and combustion step. The carbon measurements were performed on a separate magnetic sector mass spectrometer but only for combustion experiments

because of the very low carbon amounts released by stepwise crushing.

The cleanup procedure of gases released by combustion and crushing methods was identical (Verchovsky et al. 1998, 2002). First, the released gases were cryogenically separated using cryotraps cooled with liquid nitrogen, one of which was filled with a molecular sieve of 5 Å and the other, made of glass, was empty. Ar and Ne were purified using Ti–Al getters, and nitrogen was purified using a CuO furnace to ensure that no CO was present. Carbon yields (recorded as ng of C) were calculated using the pressure of CO_2 measured on a calibrated MKS Baratron™ capacitance manometer. Nitrogen and Ar yields were measured by peak height comparison with known amounts of standard gases. Gases were transferred to different parts of the machine using a system of computer-controlled pneumatic valves.

In order to reduce the contributions from CO_2^{++} and $^{40}Ar^{++}$ on Ne masses (22 and 20), a low ionization voltage of ~40 V was used in the ion source of the quadrupole mass spectrometer. Also, Ar present in the system was trapped in the molecular sieves, and the Ti–Al getter was connected to the mass spectrometer chamber during Ne measurements.

The isotopic data are expressed using the delta (δ) notation, as parts per thousand (‰) deviations from standards (Vienna Peedee Belemnite [$_{VPDB}$] for C, and terrestrial air [$_{AIR}$] for N). The system blanks were measured between sample analyses by passing an empty clean Pt foil bucket through the same stepped combustion procedure used for the sample analyses and collecting both abundance and isotopic data. Typical system blanks for stepped combustion experiments were <10 ng of C and <1 ng of N. Typical system blanks for ^{4}He were $<1 \times 10^{-8}$, for $^{20}Ne < 6.5 \times 10^{-10}$, and for ^{40}Ar and $^{36}Ar < 8 \times 10^{-9}$ and $<1.2 \times 10^{-10}$ (all in cm^3 STP), respectively. For crushing analyses, the system blanks were measured at several stages during the total sample crushing runs by stopping crushing and closing off the crushing tube for a length of time comparable to the duration of the next crushing step. Typical values were <0.76 ng of N, $<8.5 \times 10^{-9}$ cm^3 for ^{4}He, $<6 \times 10^{-9}$ cm^3 for ^{20}Ne, and for ^{40}Ar and ^{36}Ar were $<1.65 \times 10^{-8}$ cm^3 and $<3.7 \times 10^{-10}$ cm^3, respectively.

Uncertainties of absolute gas concentrations are 5–10%, and elemental noble gas ratios have estimated uncertainties of about 5%.

RESULTS AND DISCUSSION

^{40}Ar-^{39}Ar Chronology

Detailed Ar isotope data and apparent ages data for the Dhofar 1436 samples are given in Table 1.

Dhofar 1436 is a gas-rich lunar meteorite: The content of $^{36}Ar_{total}$ is 4698×10^{-8} and 3903×10^{-8} cm^3 STP g^{-1} in Dhofar 1436-a and Dhofar 1436-b, respectively, comprising >99.8 (99.5)% of $^{36}Ar_{trapped}$, assuming the trapped endmember $^{36}Ar/^{38}Ar$ ratio to be equal to 5.35 (5.47). Besides the low temperature atmospheric argon release (a usual phenomenon for desert meteorites), more than 98% of the trapped ^{36}Ar and ^{38}Ar are released at >1100 °C, just when the major simultaneous release of all other argon isotopes occurs (Figs. 1A and 1B). $^{36}Ar/^{38}Ar$ ratios in individual temperature steps >1100 °C are >5, with a maximum $^{36}Ar/^{38}Ar$ value of 5.43 ± 0.03 at 1330 °C in Dhofar 1436-a. Taking into account contribution of cosmogenic Ar to these values, the $^{36}Ar/^{38}Ar$ ratio of the trapped component must be higher. Such a high $^{36}Ar/^{38}Ar$ ratio of the trapped endmember composition implies it to be solar (5.47) rather than the nominal planetary value of 5.34 ± 0.02 (Ott 2002). In general, the $^{36}Ar/^{38}Ar$ ratios in individual temperature extractions of Dhofar 1436-a are higher than those of Dhofar 1436-b.

The Dhofar 1436 Ar release pattern is typical for impact melts and shocked meteorites. For K-Ar chronology, K-bearing phases are relevant for the release pattern of K-derived ^{39}Ar and radiogenic ^{40}Ar. Plagioclase frequently is the dominant K carrier, for example, Na-rich oligoclase in ordinary chondrites (Trieloff et al. 2003), while for differentiated rocks, more calcic plagioclase occurs, for example, of labradoritic composition in Martian shergottites, or even more calcic compositions in lunar rocks. Unshocked oligoclase (separates) from ordinary chondrites release K-derived ^{39}Ar and Ca-derived ^{37}Ar at 900 °C (Trieloff et al. 2003), at roughly the same temperature as argon release from unshocked more calcic plagioclase (Trieloff 1993). Note that the ^{39}Ar release of WR or bulk samples is dominated by plagioclase. Pyroxene, which usually contains no or only minor amounts of K, releases Ar—particularly Ca-derived ^{37}Ar—at 1300 °C.

In contrast, shocked chondrites release K-derived ^{39}Ar at much higher temperatures of >1100 °C, often as high as 1400 °C (Bogard and Hirsch 1980; Kunz et al. 1997; Trieloff et al. 2018), most likely due to shock-induced phases (shock glass, jadeite, etc.). This increase of the release temperature of K-bearing phases is also observed for the more calcic plagioclase of shergottites (Korochantseva et al. 2009), where plagioclase (maskelynite) separates were found to release both K-derived ^{39}Ar and Ca-derived ^{37}Ar at 1300–1400 °C, indistinguishable from the ^{37}Ar release from pyroxene. This explains the concomitant release of all argon isotopes at high temperatures in impact metamorphosed rocks.

Release patterns of Dhofar 1436 are quite similar to another lunar impact-melt breccia, Dhofar 280 (see Korochantseva et al. 2016) (Fig. 1C). Evidently, the simultaneous release of all argon isotopes at high temperatures in Dhofar 1436 is the consequence of shock metamorphism.

In argon three-isotope plots (Figs. 2A and 2B), the $^{40}Ar/^{36}Ar$ ratios of individual extraction steps systematically decrease from about 300 to ~2.5, thereby forming trends indicating the presence of different trapped argon components, one of which comes obviously from the terrestrial atmosphere. Therefore, the extraterrestrial trapped Ar isotopic composition cannot be accurately defined if all extraction steps are used for the line regression. However, the apparent age crucially depends on the exact isotopic composition of trapped argon (see below). Figure 3 demonstrates how the isotopic composition of the lunar trapped argon depends on the selection of individual temperature fractions. Each value of the trapped composition in Fig. 3 represents the y-axis intercept of a line fitted in the $^{39}Ar/^{36}Ar_{trapped}$ versus $^{40}Ar/^{36}Ar_{trapped}$ plot (Fig. 2) using isochron data of a temperature interval between the extraction temperature indicated by the x-axis value and 1380 °C. For example, the point at 1000 °C represents the trapped composition obtained from the fit line for extractions between 1000 °C and 1380 °C, while the data point at 1200 °C is the trapped composition obtained for the temperature extractions between 1200 °C and 1380 °C. Figure 3 shows for Dhofar 1436-a that the trapped argon compositions are virtually indistinguishable from each other only if extractions between 1100 °C and 1380 °C are selected. Adding extractions at <1100 °C results in significantly lower $^{40}Ar/^{36}Ar$ ratios for the trapped component due to contamination by atmospheric Ar. The data points in Fig. 3 show only minor variations—more pronounced for Dhofar 1436-b than for Dhofar 1436-a—and yielding a mean $(^{40}Ar/^{36}Ar)_{trapped}$ ratio of 2.51 ± 0.04, if the normal planetary trapped composition of $(^{36}Ar/^{38}Ar)_{trapped} = 5.35$ is used for deconvolution of trapped and cosmogenic ^{36}Ar. The alternative choice of $(^{36}Ar/^{38}Ar)_{trapped} = 5.47$ yields a remarkably consistent (within 1%) and virtually indistinguishable result.

The K/Ca spectra of both Dhofar 1436 subsamples show very similar variations (Fig. 4A). The age spectra are complex, displaying high apparent ages of up to >7 Ga when a standard correction for trapped primordial argon is applied (Fig. 4B). Correcting ^{40}Ar, released at the high temperature steps, by using $(^{40}Ar/^{36}Ar)_{trapped} = 2.51 \pm 0.04$, results in ages of 3.93 ± 0.15 Ga (for 51–98% cumulative ^{39}Ar release) and 4.18 ± 0.13 Ga (for 61–99% cumulative ^{39}Ar release) for Dhofar 1436-a and Dhofar 1436-b, respectively, that is, indistinguishable from each other at the 1σ level. The ages calculated by using the trapped composition $^{36}Ar/^{38}Ar = 5.47$ are almost identical to those calculated using $^{36}Ar/^{38}Ar = 5.35$. These ages with a mean value of 4.07 ± 0.12 Ga indicate that the last event, which totally reset the K-Ar system, could well be related to the period of the LHB.

The age correction for the trapped argon released at the low-temperature extractions is impossible for this desert meteorite since these fractions contain not only Ar incorporated during atmospheric transit and/or terrestrial residence but also the previously trapped extraterrestrial argon component. Hence, we cannot exclude a very recent and mild thermal event that may have induced slight diffusional losses of cosmogenic argon (see below).

Cosmic Ray Exposure (CRE) Ages

The concentrations of cosmogenic ^{38}Ar calculated using $(^{36}Ar/^{38}Ar)_{trapped} = 5.47$ yield $29.6 \pm 6.0 \times 10^{-8}$ and $29.5 \pm 5.9 \times 10^{-8}$ cm^3 STP g^{-1} in Dhofar 1436-a and Dhofar 1436-b, respectively, comprising ~3–4% of $^{38}Ar_{total}$. These concentrations are relatively high and indicate that this meteorite had a prolonged and complex CRE history and was irradiated already by GCRs on the surface of the Moon, before its transit to the Earth, which for lunar meteorites is usually <1 Ma (Nishiizumi 2004). The CRE age spectra of the samples strongly depend on the trapped endmember composition. As the $^{36}Ar/^{38}Ar$ ratios for some temperature steps extracted at $T \geq 1100$ °C exceed the planetary $(^{36}Ar/^{38}Ar)_{trapped}$ ratio of 5.35, we have chosen the solar composition of 5.47 for calculating the CRE ages (Figs. 5A–D), which is similar to the maximum value of 5.43 ± 0.03 observed in the high temperature steps of Dhofar 1436 samples (1330 °C in Dhofar 1436-a). Similarly, high values of 5.40 ± 0.01 are also measured by the stepwise crushing extractions (Tables 2 and 3). Assuming negligible contribution of 4π irradiation, the minimum irradiation time on the Moon is calculated from the maximum P_{38} of 13.77×10^{-10} cm^3/g^{-1}Ma for a shielding depth of 65 g cm^{-2} by the model of Hohenberg et al. (1978) for 2π irradiation (Figs. 5A and 5C). The CRE ages indicate that the meteorite accumulated $^{38}Ar_{cos}$ by GCR irradiation on the lunar surface during long period(s) of time. However, the error bars are large due to the high amount of trapped solar wind argon. Systematic errors concerning production rates and the exact composition of the solar wind $^{36}Ar/^{38}Ar$ endmember composition are neglected. We prefer the lower bound of the error bars as an approximation for a CRE age of larger than 200 Ma (for >23% of the fractional ^{37}Ar release,

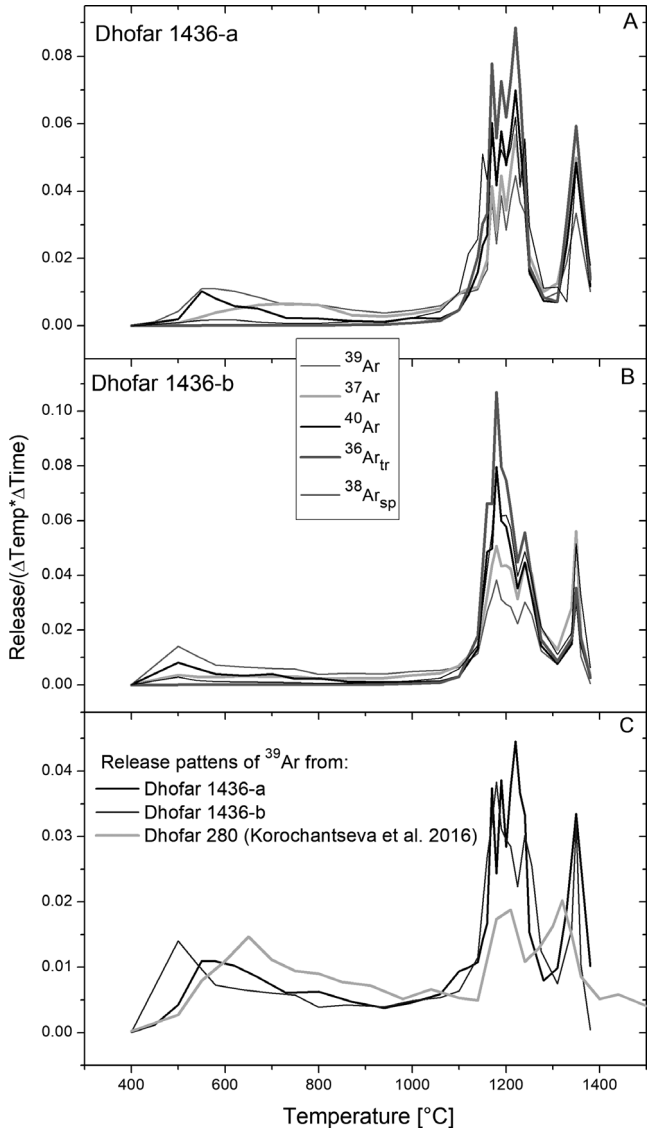

Fig. 1. Release patterns of argon isotopes of Dhofar 1436 samples (A, B). $^{36}Ar_{trapped}$ is calculated with $(^{36}Ar/^{38}Ar)_{trapped} = 5.47$ and $(^{36}Ar/^{38}Ar)_{cos} = 0.65$. The major release of argon isotopes is above 1100 °C. The ^{39}Ar release patterns of Dhofar 1436 specimens are similar to that of another lunar impact breccia Dhofar 280 (C).

Figs. 5A and 5C) and we will further evaluate this value using the concentration of cosmogenic neon below. Note that Dhofar 1436 releases cosmogenic gases that accumulated both before and after the 4.1 ± 0.1 Ga event. However, those that accumulated before are more abundant (see the Noble Gas Elemental Ratios section). Furthermore, the CRE age spectra indicate diffusional loss of $^{38}Ar_{cos}$ at the first ~30% of ^{37}Ar release, similar to what has been observed for Dhofar 280 (Korochantseva et al 2016). In the case of Dhofar 280, this part of the CRE age spectrum with diffusional loss allowed us to calculate both the irradiation period on the Moon as well as the transit time to Earth. Applying a similar reasoning to Dhofar 1436 seems not to be appropriate: If the 4π irradiation production rate of 22.09×10^{-10} cm^3/g^{-1}Ma (Eugster and Michel 1995) is used for the Dhofar 1436 samples for the low temperature steps (Figs. 5B and 5D), a CRE maximum transit age of 14 Ma is inferred (Fig. 5B), which is nevertheless a rather unrealistically long transit time for lunar meteorites (Nishiizumi 2004). Hence, it is more likely that cosmogenic nuclides have been partially retained during the most recent partial degassing event or/and that the meteorite was irradiated on the lunar surface after the major impact event at 4.1 ± 0.1 Ga ago. If the 2π irradiation production rate of 13.77×10^{-10} cm^3/g-1Ma (Hohenberg et al. 1978) is used for the low temperature steps of Dhofar 1436 samples (Figs. 5B and 5D), a CRE minimum age of 24 Ma is obtained for the recent (post 4.1 Ga) exposure (see discussion below).

Ne data obtained by the stepped combustion experiment at The Open University (Table 4) can also be used to determine the CRE age of Dhofar 1436 using the total amount of $^{21}Ne_{cos} = 920 \times 10^{-10}$ cm^3 STP g^{-1} (calculated applying the endmember compositions of SW Ne with $^{20}Ne/^{22}Ne = 13.78$ and $^{21}Ne/^{22}Ne = 0.0329$; Heber et al. 2009) and cosmogenic Ne with $^{20}Ne/^{22}Ne = 0.8$ (Eugster and Michel 1995) and $^{21}Ne/^{22}Ne = 0.86$ (the average value for the $(^{21}Ne/^{22}Ne)_{cos}$ range, See the Noble Gases: Release, Abundances, Isotopic Compositions section. We calculate a lunar surface exposure of 94 Ma using $P_{21} = 9.75 \times 10^{-10}$ cm^3/g^{-1} Ma and a shielding depth of 65 g cm^{-2} by the model of Hohenberg et al. (1978) for 2π irradiation. Taking into account that the meteorite experienced diffusional loss of cosmogenic noble gases and assuming further that diffusive losses for Ne were more pronounced than for Ar, this age is in good agreement with the CRE age estimate obtained by ^{40}Ar-^{39}Ar analyses and also indicates a significant—though not exceptionally long—irradiation time on the Moon.

Noble Gases: Release, Abundances, Isotopic Compositions

The stepwise crushing and combustion results for the noble gas abundances and isotopic compositions of the Dhofar 1436 samples are listed in Tables 2–6.

The stepwise combustion of the WR sample Dhofar 1436-e demonstrates distinct release peaks of He, Ne, and Ar (at 900, 1200, and 1300 °C, respectively) due to their different diffusion rates (Fig. 6). The powdered samples display much lower peak release temperatures for these gases, which can be explained by facilitated

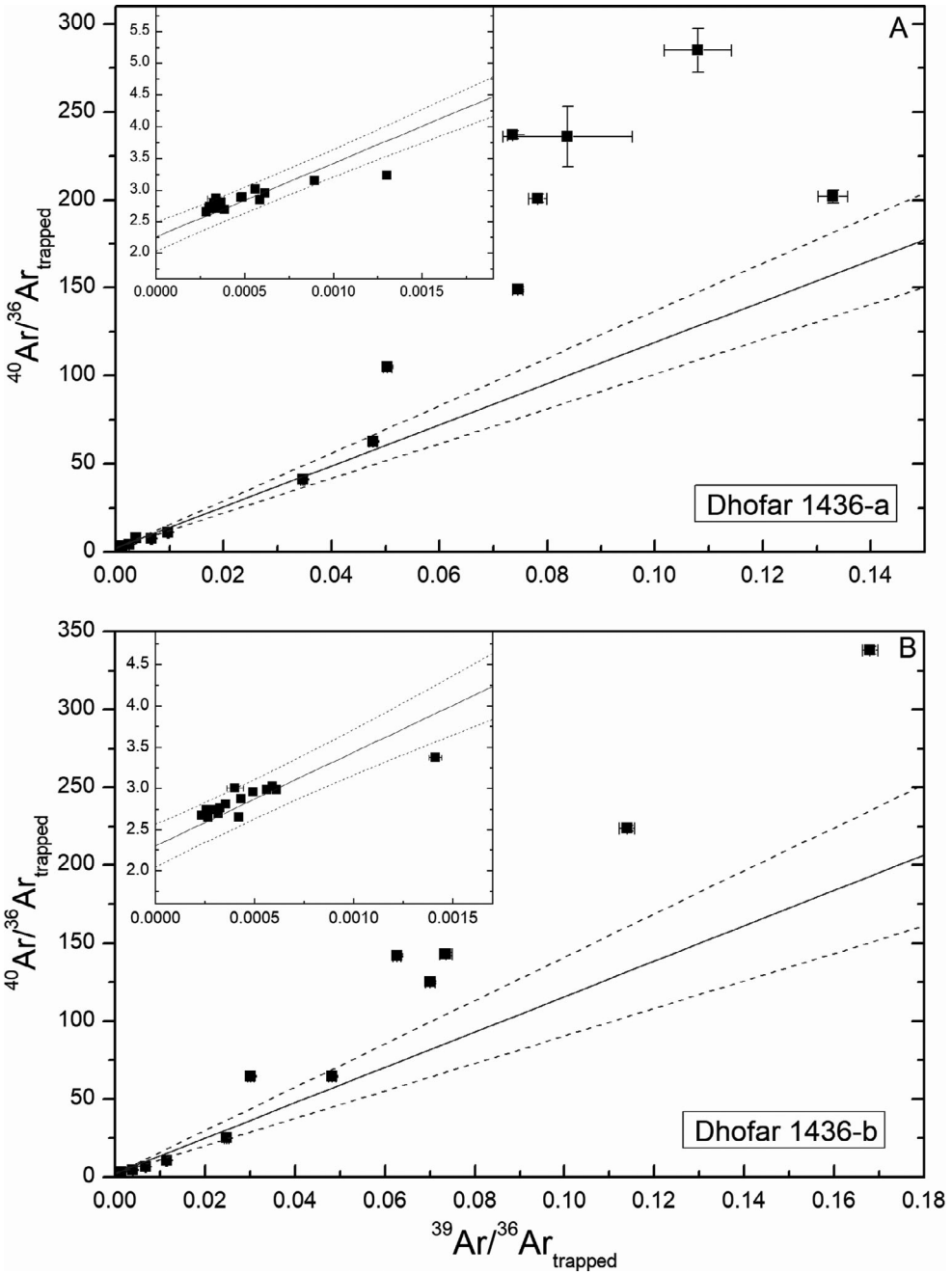

Fig. 2. Isochron plots of $^{40}Ar/^{36}Ar_{trapped}$ versus $^{39}Ar/^{36}Ar_{trapped}$ ratios for Dhofar 1436 samples. The data points form a trend, indicating the presence of extraterrestrial trapped components. Isochron plots are for $(^{36}Ar/^{38}Ar)_{tr} = 5.35$, however, using 5.47 yield nearly indistinguishable results. The regression lines were calculated applying the error weighted least squares method.

gas diffusion from the crushed fine-grained material. Fractionation between different noble gases still persists in the powdered material. In particular, the powdered specimen recovered after the intensive crushing carried out at The Open University (OU) shows release peaks of He, Ne, and Ar at 300, 700, and 800 °C, respectively (Fig. 6).

During crushing, noble gases are mostly released in the initial steps. Afterward the efficiency of noble gases release, defined as the amount of noble gas released per stroke, sharply decreases (Tables 2 and 3). The amounts of ^{4}He, ^{20}Ne, and ^{36}Ar of 569, 48, and 44 ($\times 10^{-6}$ cm^3 STP g^{-1}) released by prolonged crushing (totally 12,100 strokes) at the OU accounts for 93, 86, and 76% of the

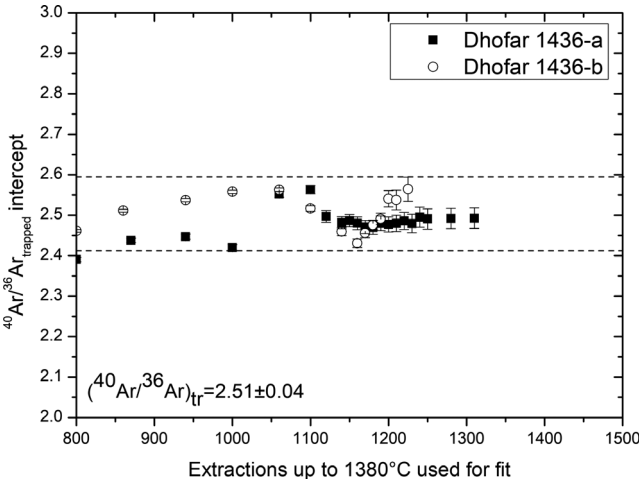

Fig. 3. Dependence of the lunar trapped argon composition on the selection of temperature extractions. The shown data points, except for the first one of Dhofar 1436-a, fall into the interval 2.51 ± 0.08, which corresponds to a 2–3σ error. The inferred value is 2.51 ± 0.04.

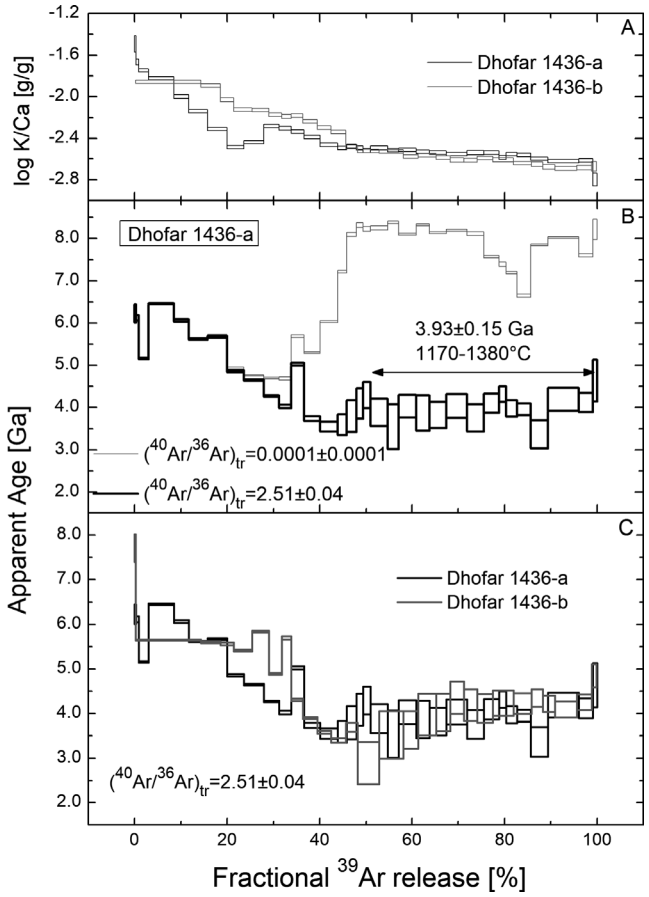

Fig. 4. K/Ca spectra (A) and age spectra (B, C) of Dhofar 1436 samples before and after correction for a lunar trapped component with $(^{40}Ar/^{36}Ar)_{trapped}$ = 2.51 ± 0.04. The "uncorrected" age spectrum contains a nominal routine correction for primordial argon with $(^{40}Ar/^{36}Ar)_{trap}$ = 0.0001 ± 0.0001 (Göbel et al. 1978).

total amounts extracted by crushing and subsequent combustion of the remaining powder, respectively. The crushing analyses (totally 5000 strokes) at the University of Heidelberg (HD) extracted 34, 19, and 11 ($\times 10^{-6}$ cm^3 STP g^{-1}) of ^{4}He, ^{20}Ne, and ^{36}Ar, respectively. The apparent discrepancy in gas amounts of these samples as well as of Dhofar 1436-e (see Table 4) could be due to sample heterogeneity of the material of the Dhofar 1436 breccia. As alternative explanation, during sample preparation and fragmentation, some ^{4}He may have been lost, as most of the helium is released in the first crushing steps.

In the initial crushing steps, ^{4}He/^{3}He ratios correspond to the solar wind (SW) value and ^{20}Ne/^{22}Ne ratios are up to 12.57 (Table 2). The Ne isotopic compositions of all samples analyzed are shown in the neon three-isotope diagram (Fig. 7). The Ne data for the HD crushing experiments form a trend, reflecting the dependence of isotopic composition of released Ne on the strength of voids/inclusions against crushing and showing increase of the ^{21}Ne/^{22}Ne ratio with decreasing ^{20}Ne/^{22}Ne ratio. Similar trends for Ne have been observed during crushing of the Pesyanoe aubrite samples (Buikin et al. 2013, 2015) and the Ghubara meteorite (L5; Korochantseva et al. 2018). These trends are very similar to the curve obtained for stepwise etching of Apollo samples (Wieler et al. 1986; see Fig. 8A), reflecting a mixture of depth-dependent implantation-fractionated solar wind (FSW) and the cosmogenic component (e.g., Grimberg et al. 2006). Moreover, the same trend can be found for stepwise heating data of lunar meteorites (Eugster et al. 1992, 1996) (see Fig. 8B). Regardless of the method, all studies indicate that cosmogenic Ne is a more retentive component than solar Ne. In comparison, Dhofar 1436 data form a curved function with various contributions from trapped and cosmogenic neon, the latter more pronounced at the late crushing steps (Fig. 8). Hence, we can conclude that the former component is mostly released from relatively large voids destroyed in the initial crushing steps, while cosmogenic nuclides are extracted from smaller ones at the end of crushing. The relative contributions of cosmogenic ^{20}Ne and ^{21}Ne in the Dhofar 1436-c sample (crushed at HD) calculated using the endmember compositions of SW Ne with ^{20}Ne/^{22}Ne = 13.78 and ^{21}Ne/^{22}Ne = 0.0329 (Heber et al. 2009) and cosmogenic Ne with ^{20}Ne/^{22}Ne = 0.8 (Eugster and Michel 1995) and ^{21}Ne/^{22}Ne = 0.86 (the average value for the $(^{21}Ne/^{22}Ne)_{cos}$ range, see Fig. 8A) are <1 and ~29%, respectively. At the late crushing

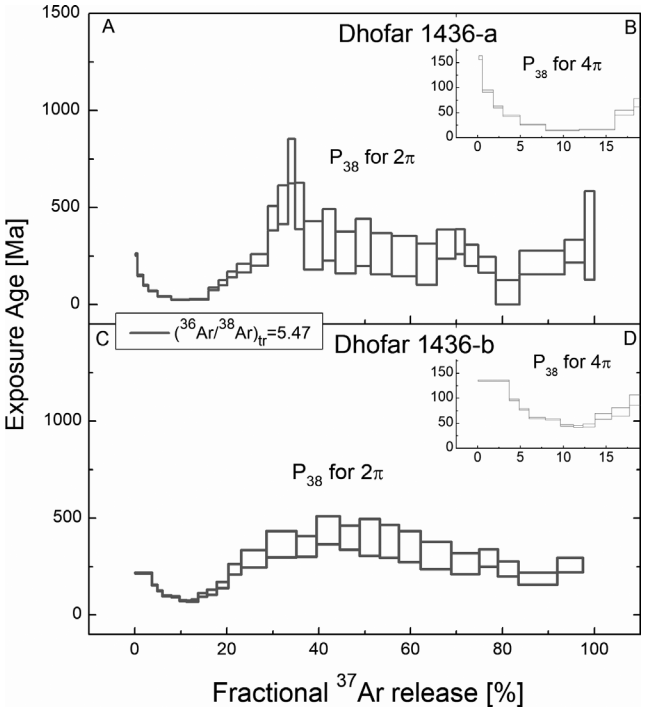

Fig. 5. Cosmic ray exposure age spectra of Dhofar 1436 samples calculated using solar $(^{36}Ar/^{38}Ar)_{trapped}$ ratio of 5.47. Spectra are calculated from the maximum P_{38} of 13.77×10^{-10} $cm^3/g^{-1}Ma$ for the shielding depth of 65 g cm^{-2} given by the model of Hohenberg et al. (1978) for 2π irradiation and, hence, show the minimum irradiation time on the Moon. CRE ages with the production rate for 4π irradiation indicate diffusional loss of $^{38}Ar_{cos}$ in the beginning of the CRE spectra (small insets).

steps, the contribution of cosmogenic components comprises up to 1.4 and 52% of $^{20}Ne_{total}$ and $^{21}Ne_{total}$, respectively.

At first sight, it seems somewhat surprising that solar wind implanted noble gases as well as cosmogenic gases can be extracted not only by heating but also by crushing, and—moreover—can be separated by stepwise crushing in a similar manner than by stepwise heating. A first ad hoc explanation could be that the radiation-damaged grain boundaries hosting solar wind implanted gases represent noble gas trapping sites that are easily accessible by both mild crushing and also heating, while the much less radiation-damaged interior rock domains hosting cosmic ray induced spallation products form trapping sites that require stronger crushing and/or heating to release cosmogenic noble gases. The view that solar wind gases are still located and extracted from the unaltered original grain boundaries in which they once were implanted may be seriously oversimplified and incorrect, as argued below.

Concerning the mere feasibility of extracting cosmogenic noble gases by crushing, this was already confirmed by several studies on mantle rocks (Hilton et al. 1993; Scarsi 2000; Moreira and Madureira 2005; Yokochi et al. 2005), showing that the cosmogenic atoms (in particular, He and Ne), which formed within tracks of the mineral matrix can be extracted during crushing. According to Yokochi et al. (2005) and Moreira and Madureira (2005), solid-state volume diffusion is not able to extract helium and neon during crushing because of their low diffusivity in mafic minerals at the low crushing temperature that does not exceed 70 °C. The authors consider that spallation damage tracks along fractures may provide sufficient pathways for He and Ne extraction by prolonged crushing. The diffusion of gases located in the mineral crystalline lattice cannot be completely ruled out during crushing, since locally, on a micrometer scale, the temperature could rise significantly as a result of grain collisions when the crushing energy is released within a small volume. Another possibility was raised by Bekaert et al. (2018) who considered recoil of cosmogenic gases into vesicles as an additional explanation.

The plot of $^4He/^3He$ versus $^{21}Ne/^{22}Ne$ shows a trend (Fig. 9) that can be explained by a mixture of solar-like and cosmogenic components, where the relative contribution of the latter increases with progressive crushing. The Dhofar 1436-c sample crushed at HD contains ≤0.1 and ~16% of cosmogenic ^4He and ^3He of the total amounts of these isotopes, respectively, calculated using the endmember $^3He/^4He$ ratios for SW and cosmogenic components of 4.64×10^{-4} (Heber et al. 2009) and 0.12–0.23 (Reimer et al. 1998; Wieler 2002), respectively.

The $^{36}Ar/^{38}Ar$ ratios of the Dhofar 1436-d sample crushed at the OU are within the range 5.31–5.40 and slightly decrease in the final crushing steps (Table 3). These $^{36}Ar/^{38}Ar$ ratios are close to almost pure trapped solar argon with small, if any, cosmogenic contributions, in contrast to what is observed for He or Ne. This is quite unexpected as solar wind is normally depleted in heavy noble gases relative to light ones when compared to planetary (or cosmogenic) components. However, the elemental ratio $^{20}Ne/^{36}Ar$, which is within the range between 1 and 2, clearly demonstrates that the solar wind component in this sample is elementally fractionated, a conclusion that will be further discussed below. The heated powder obtained after intensive crushing at OU obviously contains less trapped gases, showing lower $^{36}Ar/^{38}Ar$ ratios (4.44–4.59), while the heated WR sample gives intermediate values between 4.6 and 5.1. The $^{36}Ar_{cos}$ and $^{38}Ar_{cos}$ (released by crushing in HD and at the OU) calculated using $(^{36}Ar/^{38}Ar)_{SW} = 5.47$ (Heber et al.

Table 3. Data on noble gases (He, Ne, and Ar) and N_2 for Dhofar 1436-d by stepwise crushing at the OU (19.78 mg).

Extractions[a]	^4He[b]	^{20}Ne[b]	$^{20}Ne/^{22}Ne$	$^{21}Ne/^{22}Ne$	^{36}Ar[b]	$^{40}Ar/^{36}Ar$	$^{36}Ar/^{38}Ar$	$^4He/^{20}Ne$	$^{20}Ne/^{36}Ar$	N[c]	$\delta^{15}N$[d]
10	29703.4	1151.9	11.77 (7)	0.0433 (13)	158.2	10.3	5.33	25.8	7.28	670.0	−12.1 (1.5)
50	467.3	605.5	11.29 (3)	0.0450 (7)	250.4	4.4	5.35	0.8	2.42	325.9	−23.2 (1.6)
200	1034.2	610.9	11.19 (3)	0.0453 (7)	515.2	3.5	5.40	1.7	1.19	545.5	−31.6 (1.5)
500	1454.7	379.4	11.26 (4)	0.0477 (10)	539.8	3.2	5.40	3.9	0.70	439.9	−36.3 (1.4)
1100	2144.6	316.0	11.40 (5)	0.0506 (10)	607.1	3.3	5.40	6.8	0.52	468.4	−36.0 (1.5)
2100	2802.4	275.8	11.36 (5)	0.0500 (12)	574.1	3.1	5.40	10.2	0.48	384.4	−36.1 (1.5)
4100	4126.9	358.6	11.30 (4)	0.0461 (9)	604.0	3.1	5.37	11.5	0.59	250.0	−33.9 (1.5)
6100	3664.8	305.7	11.35 (5)	0.0414 (10)	403.6	3.2	5.37	12.0	0.76	75.4	−30.8 (2.4)
8100	3475.6	264.8	11.30 (5)	0.0390 (9)	234.8	3.2	5.32	13.2	1.13	24.8	−22.3 (3.0)
10100	3881.8	269.1	11.38 (5)	0.0392 (10)	274.1	3.0	5.37	14.5	0.98	10.9	3.8 (4.1)
12100	4109.7	267.5	11.39 (5)	0.0372 (10)	249.2	2.9	5.31	15.4	1.07	4.3	−2.1 (5.9)
Total	56863.7	4805.2	11.41 (5)	0.0446 (10)	4410.4	3.5	5.38	11.86	1.09	3199.6	−28.4 (1.6)

5–10% uncertainty in absolute concentrations of noble gases.
Numbers in parentheses refer to the last digits and are 1σ-uncertainties.
Uncertainties for $^{40}Ar/^{36}Ar$ and $^{36}Ar/^{38}Ar$ are 0.1 and 0.01, respectively.
[a]Cumulative number of strokes.
[b]$\times 10^{-8}$ cm^3 STP g^{-1}.
[c]ppb.
[d]‰.

2009) and $(^{36}Ar/^{38}Ar)_{cos} = 0.65$ (Eugster et al. 1991) is 0.2 and 1.9% of the total amounts of the isotopes, respectively. The result is consistent with the value obtained from Ar-Ar dating. The $^{40}Ar/^{36}Ar$ ratios of the crushed samples range between 2 and 3 (except for just the first one to two extraction steps contaminated with atmospheric Ar; see Tables 2 and 3), in agreement with the $(^{40}Ar/^{36}Ar)_{trapped}$ ratios obtained by the ^{40}Ar-^{39}Ar analysis and noble gas stepwise combustion.

Lunar Trapped Orphan Argon

In Dhofar 1436, the trapped argon with $^{40}Ar/^{36}Ar$ ratios of ~2–3 has solar-like $^{36}Ar/^{38}Ar$ ratios. This indicates that ^{36}Ar is ultimately of solar wind origin. The consistency of the $^{40}Ar/^{36}Ar$ values found for all analyses indicates that $^{36}Ar_{solar}$ is intimately associated with an excess of radiogenic ^{40}Ar far higher than the solar wind $^{40}Ar/^{36}Ar$ ratio of 0.0001 ± 0.0001 (e.g., Göbel et al. 1978; Wieler and Heber 2003, and references therein).

A widely accepted mechanism to explain the "orphan" excess ^{40}Ar is a process suggested by Heymann and Yaniv (1970) and Manka and Michel (1971), which implies escape of ^{40}Ar into the lunar atmosphere, uptake by the solar wind, and reimplantation into the rocks and minerals exposed on the lunar surface. However, already in the 1970s, several studies pointed to problems with this mechanism (Baur et al. 1972; Heymann and Kirsten 1973; Bernatowicz et al. 1980). A major problem was related to the low implantation energy of ^{40}Ar of about 1 keV versus ^{36}Ar of about 30 keV (e.g., Baur et al. 1972; Heymann and Kirsten 1973), which should result in differential release during stepwise heating (a few 100 °C peak difference, see Baur et al. 1972). However, most studies found a perfect coherence during stepwise heating (e.g., Baur et al. 1972; see also Bernatowicz et al. [1980], and Mortimer et al. [2016]). This led Baur et al. (1972) to conclude "... will require reexamination of theories which ascribe" orphan "^{40}Ar to a low energy retrapping of ^{40}Ar from the lunar atmosphere" and "In conclusion we suggest that the retrapping of ^{40}Ar from the lunar atmosphere as proposed by Heymann et al. (1970) is not the only source of orphan Ar."

A possible solution for this problem was discussed by Heymann and Kirsten (1973). They assumed that—although trapped gases were originally acquired during surface irradiation by solar wind—they could no longer reside in the "radiation-damaged outer skin of fines particles (50 nm thick), but ... in the less damaged, deeper regions," possibly 8 nm sized bubbles identified by Phakey et al. (1972), in which they had been transferred during agglutination. It should be noted that during (impact induced) rapid compaction at elevated temperatures, grains should be first compressed—some aggregates or subunits may show closed, others open porous structures thereby allowing gases from grain boundaries to escape partially and fractionate. Almost simultaneous should be the sintering of grain

Table 4. Stepwise combustion data for the whole rock sample Dhofar 1436-e (3.117 mg).

T (°C)	$^{4}He^{a}$	$^{20}Ne^{a}$	$^{20}Ne/^{22}Ne$	$^{21}Ne/^{22}Ne$	$^{36}Ar^{a}$	$^{40}Ar^{a}$	$^{36}Ar/^{38}Ar$	N^{b}	$\delta^{15}N^{c}$	C^{d}	$\delta^{13}C^{c}$
200	b.d.	b.d.	n.a.	n.a.	0	379.6	n.a.	1024.4	−7.8 (4)	b.d.	n.a.
300	191.1	6.4	n.a.	n.a.	b.d.	134.1	n.a.	3111.0	−0.5 (3)	137.7	−22.0 (2)
400	415.7	15.0	n.a.	n.a.	b.d.	51.4	n.a.	2931.3	0.0 (3)	156.7	−23.8 (2)
500	986.7	52.9	n.a.	n.a.	0.7	14.7	n.a.	2140.6	−2.6 (3)	71.0	−18.2 (3)
600	1895.7	168.8	11.43 (21)	0.0410 (43)	3.4	29.7	n.a.	1188.5	−16.0 (4)	84.7	−5.0 (6)
700	2185.8	367.7	11.78 (15)	0.0472 (31)	5.9	b.d	4.65 (6)	980.2	−6.2 (5)	47.5	1.4 (5)
800	3488.7	654.4	11.84 (11)	0.0469 (21)	15.3	b.d.	5.03 (3)	534.5	−6.4 (7)	9.6	−11.5 (6)
900	3910.7	867.6	11.83 (10)	0.0490 (17)	26.3	b.d.	4.69 (1)	480.5	−6.1 (8)	5.3	−17.3 (4)
1000	2221.6	1045.5	11.76 (9)	0.0458 (17)	19.4	b.d.	4.61 (1)	n.a.	n.a.	2.9	−10.0 (8)
1100	909.0	1084.4	11.75 (9)	0.0454 (16)	30.3	b.d.	4.81 (1)	n.a.	n.a.	3.2	−12.3 (7)
1200	210.8	3272.1	11.40 (5)	0.0444 (10)	1965.4	4961.4	5.10 (1)	2844.9	−79.4 (4)	10.5	11.1 (8)
1300	146.8	468.4	11.59 (12)	0.0504 (26)	2976.8	8150.0	5.03 (1)	2852.3	−76.5 (4)	11.8	5.8 (4)
1400	166.8	11.2	n.a.	n.a.	446.3	1348.8	4.78 (1)	847.7	−34.5 (4)	4.4	−6.1 (5)
1430	b.d.	b.d.	n.a.	n.a.	b.d.	b.d.	n.a.	307.8	−10.6 (1.1)	2.8	−15.7 (1.6)
1460	b.d.	8.4	n.a.	n.a.	b.d.	34.2	n.a.	1593.6	−2.1 (3)	7.1	−28.4 (2)
Total	16729.4	8022.9	11.60 (8)	0.0459 (16)	5489.6	15104.1	5.03 (1)	20837.3	−25.3 (4)	555.3	−15.8 (4)

5–10% uncertainty in absolute concentrations of noble gases.
Numbers in parentheses refer to the last digits and are 1σ-uncertainties.
b.d. = below detection limit; n.a. = not analyzed.
[a]$\times 10^{-8}$ cm^3 STP g^{-1}.
[b]ppb.
[c]‰
[d]ppm.

boundaries leading to further compaction and solidification, thereby former grain boundaries encapsulate partly vesicular/porous interiors of the compacted breccia, in which the former surface correlated noble gases become trapped. Small vesicular cavities have also been observed by Noguchi et al. (2014), who considered blistering during solar wind implantation of helium on some Itokawa particles. However, they noted that these vesicles were much smaller than those in the rims of lunar regolith breccias described by Noble et al. (2005). The authors of the last study described cavity sizes of 100–200 nm within the vesicular and glassy rims, which were assumed to have formed in situ by heating during the lithification processes, because lunar soils usually lack such rim types (Noble et al. 2005).

Imagining that surfaces of agglutinating grains could form traps (e.g., very small vesicles) upon heating by agglutination, could explain (1) why solar wind isotopes are strongly bound in the interior of rocks, (2) why ^{36}Ar and ^{40}Ar behave coherently (diffusion is governed by vesicle strength or diffusion path through the minerals, not any more by implantation energy), (3) why these former solar wind noble gases are strongly fractionated (by heating and partial loss during agglutination, see later section and Fig. 10), and (4) why these noble gases can be extracted by stepwise crushing.

So it seems reasonable to assume that some energetic process is needed (for agglutination, trapping, equilibration) in addition to solar wind implantation. Impact-induced heating, possibly also solar heating, is a viable energy source (see Shuster and Cassata [2015] for effects ascribed to solar heating). However, in our opinion, mild solar heating would rather result in the preferential extraction of the (1 keV implanted) ^{40}Ar and would not have the capacity to lock both ^{40}Ar and ^{36}Ar into more retentive non-surface sites. We think that impact heating is a much stronger and effective heat source to cause agglutination and to lock both isotopes into more retentive traps. Considering these scenarios, it is quite evident that during laboratory heating trapped gases are not extracted from the original surfaces in which they had been once implanted.

It is also interesting that some lunar soil samples exhibit main Ar release at 600–800 °C (Mortimer et al. [2016], similar to Baur et al. 1972), while some other lunar rocks release solar wind implanted argon at temperatures as high as 1200–1500 °C. From studying meteorites and lunar rocks, the high release temperature seems to be due to shock modifications of the rocks (e.g., Bogard and Hirsch 1980; Kunz et al. 1997), as it is likely the case for our sample Dhofar 1436. We therefore assume that strong shock metamorphism locked gases in these highly retentive sites.

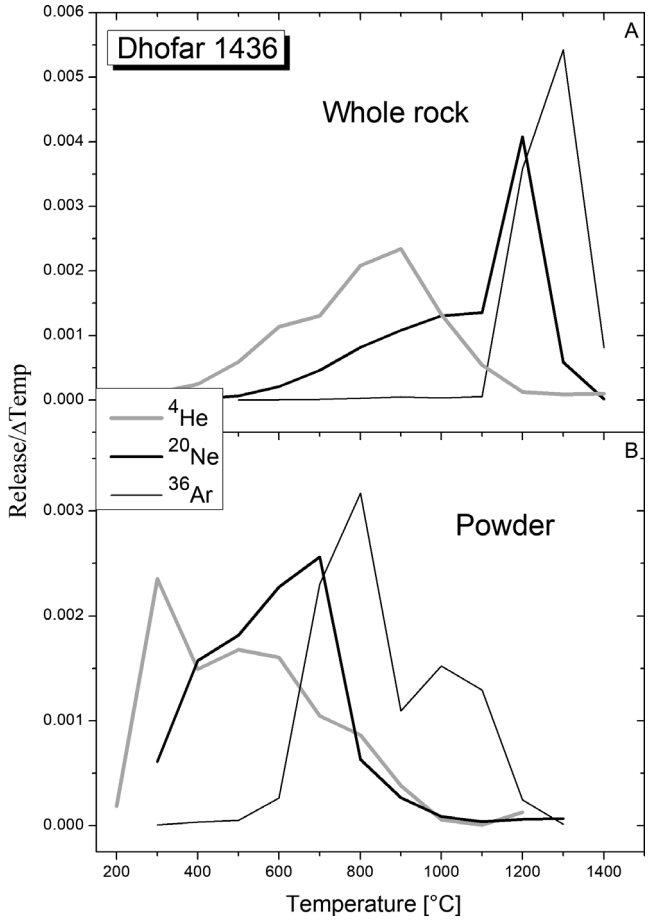

Fig. 6. ^{4}He, ^{20}Ne, and ^{36}Ar degassing patterns of whole rock and of residual powder after intensive crushing carried out at the OU. Distinct release peaks of He, Ne, Ar, and facilitated gas diffusion from crushed material are observed.

Concerning the determination of the trapped $^{40}Ar/^{36}Ar_{trapped}$ composition via ^{40}Ar-^{39}Ar dating and associated isochron plots, it is also important to note that the event that trapped surface sited ^{40}Ar and ^{36}Ar into deeper sites should also have the power to reset the K-Ar system, that is, degas preexisting radiogenic ^{40}Ar. If the precursor soil or rock was not reset (and consisted of protoliths or fragments of different ages), it would be impossible to obtain a straight line in an isochron plot, unless the precursor protoliths accidentally had all the same age.

It is furthermore likely that the same energetic process that tightly traps solar wind gases (in sites that degas only at high temperatures but that are nevertheless accessible by crushing) could not only mobilize preexisting in situ radiogenic ^{40}Ar but could also equilibrate this component. That such a process exists can be demonstrated by studies which found trapped argon with $^{40}Ar/^{36}Ar_{trapped}$ of ≥30, 37, and ~100 in lunar rocks 15426 (Huneke et al. 1973), 76535 (Bogard et al. 1975), and 67618 (Schaeffer and Schaeffer 1977), respectively. Such values must contain a redistributed in situ radiogenic ^{40}Ar component, as these values are far above reasonable solar wind mixtures of ^{36}Ar and ^{40}Ar captured from the lunar atmosphere. Such trapped argon components are also known from non-lunar meteorites that originated from Mars, Vesta, and other asteroids (Korochantseva et al. 2017; Trieloff et al. 2018).

Based on the presence of ^{40}Ar retrapped or reimplanted from the lunar atmosphere by the solar wind, Eugster et al. (2001) suggested using the $(^{40}Ar/^{36}Ar)_{trapped}$ ratio as a measure for the antiquity of surface exposure. They argued that $^{40}Ar/^{36}Ar_{trapped}$ was higher during early exposure, as there was more ^{40}Ar produced by ^{40}K-decay and because the early active Moon released ^{40}Ar more effectively into the lunar atmosphere. Eugster et al. (2001) included three points in their calibration curve representing ^{40}Ar-^{39}Ar ages and their $(^{40}Ar/^{36}Ar)_{trapped}$. They already assigned these points as less reliable and noted the problem that ^{40}Ar-^{39}Ar ages might not necessarily correspond to the time of irradiation of these rocks.

In the case of our Dhofar 1436 sample, we may specifically discuss the timing of Ar trapping and breccia solidification. Samples Dhofar 1436-a and Dhofar 1436-b contain different lithic fragments and are distinct in the proportion of matrix and clastic material. Nevertheless, Ar-Ar analyses of both subsamples yield a 4.1 Ga isochron due to mixture of a radiogenic component and a trapped solar wind component which appears homogeneous throughout the Dhofar 1436 breccia. Hence, Dhofar 1436 must have experienced a high grade event degassing all preexisting in situ radiogenic ^{40}Ar accumulated before 4.1 Ga ago. In a first possible scenario, trapped argon with $(^{40}Ar/^{36}Ar)_{trapped} = 2.5$ or lower may have been acquired before, partially lost, but also equilibrated during this high grade event, and, most importantly, was transferred into more retentive interior sites/traps by agglutination, grain boundary sintering, and vesicle formation. Trapped argon may then comprise both solar wind (including reimplanted ^{40}Ar) and preexisting radiogenic ^{40}Ar. This scenario would explain many features by assuming a single 4.1 Ga impact event that transformed a loosely packed soil into a relatively solid breccia.

Alternatively, irradiation and SW implantation occurred after the 4.1 Ga event. In this scenario, the 4.1 Ga event only reset the K-Ar system but did not cause breccia formation. Instead, it left the soil relatively loosely agglomerated (otherwise, solar wind could not be implanted throughout the many grains

Table 5. Stepwise combustion data for Dhofar 1436-c-p (powdered sample) retained after Heidelberg crushing (2.049 mg).

T (°C)	$^{4}He^{a}$	$^{20}Ne^{a}$	$^{20}Ne/^{22}Ne$	$^{21}Ne/^{22}Ne$	$^{36}Ar^{a}$	$^{40}Ar/^{36}Ar$	$^{36}Ar/^{38}Ar$	N^{b}	$\delta^{15}N^{c}$	C^{b}	$\delta^{13}C^{c}$
200		b.d.	n.a.	n.a.	b.d.	n.a.	n.a.	10.4	0.2 (7)	375	−27.4 (3)
300	330	57	n.a.	n.a.	12	13.1	n.a.	55.3	11.3 (6)	1200	−27.1 (1)
400	402	137	11.52 (11)	0.0346 (23)	20	4.60	n.a.	26.8	5.9 (5)	928	−24.2 (3)
500	457	154	11.28 (11)	0.0322 (23)	b.d.	n.a.	n.a.	17.6	4.2 (6)	789	−19.3 (3)
600	553	165	11.28 (9)	0.0308 (20)	b.d.	n.a.	n.a.	5.79	2.6 (7)	571	−3.7 (1)
700	855	178	10.62 (9)	0.0377 (23)	140	1.50	4.91 (2)	5.24	2.3 (7)	65	−22.9 (4)
800	1610	143	10.43 (8)	0.0396 (26)	413	2.08	4.92 (2)	7.75	−0.6 (8)	98	−20.4 (2)
900	1970	204	10.97 (8)	0.0366 (20)	586	2.19	4.88 (2)	8.28	−3.3 (8)	80	−20.6 (4)
1000	1120	211	11.19 (8)	0.0346 (17)	413	1.88	4.84 (2)	6.00	−3.6 (7)	45	−16.2 (2)
1100	513	114	n.a.	n.a.	635	2.03	4.91 (2)	3.06	−4.7 (6)	39	−17.6 (3)
1200	930	58	n.a.	n.a.	1540	2.84	4.90 (2)	3.75	−16.7 (6)	28	−14.6 (4)
1300	236	19	n.a.	n.a.	441	2.40	4.74 (2)	1.44	−19.9 (9)	13	−18.2 (2)
1400	289	24	n.a.	n.a.	267	2.73	4.65 (2)	0.917	−29.3 (1.6)	7	−22.6 (1)
1450	b.d.	b.d.	n.a.	n.a.	b.d.	n.a.	n.a.	0.349	−25.8 (3.1)	3	−33.2 (3)
Total	9265	1465	11.03 (9)	0.0355 (22)	4466	2.42	4.86 (2)	152.7	4.5 (6)	4240	−21.2 (2)

5–10% uncertainty in absolute concentrations of noble gases.
Numbers in parentheses refer to the last digits and are 1σ-uncertainties.
Uncertainties for $^{40}Ar/^{36}Ar$ are 0.1.
b.d. = below detection limit; n.a. = not analyzed.
[a] $\times 10^{-8}$ cm^3 STP g^{-1}.
[b] ppm.
[c] ‰

Table 6. Stepwise combustion data for Dhofar 1436-d-p (powdered sample) retained after OU crushing (4.957 mg).

T (°C)	$^{4}He^{a}$	$^{20}Ne^{a}$	$^{20}Ne/^{22}Ne$	$^{21}Ne/^{22}Ne$	$^{36}Ar^{a}$	$^{40}Ar^{a}$	$^{36}Ar/^{38}Ar$	N^{b}	$\delta^{15}N^{c}$	C^{b}	$\delta^{13}C^{c}$
200	166.0	b.d.	n.a.	n.a.	b.d.	0.7	n.a.	2.8	−1.3 (4)	234.4	−29.7 (3)
300	1053.2	49.7	n.a.	n.a.	0.9	b.d.	n.a.	20.6	1.6 (3)	942.0	−19.9 (3)
400	667.5	127.3	11.71 (22)	0.0331 (34)	4.9	84.2	n.a.	20.0	5.8 (3)	1453.5	−23.8 (3)
500	751.1	147.0	11.36 (20)	0.0345 (32)	7.1	27.2	n.a.	19.9	7.0 (4)	495.3	−21.5 (3)
600	717.3	184.2	11.75 (16)	0.0391 (32)	36.4	114.4	4.44	8.0	4.3 (4)	151.3	−17.3 (3)
700	468.6	207.3	11.57 (16)	0.0383 (30)	318.1	1001.6	4.59	34.9	−3.8 (4)	188.9	−25.3 (3)
800	387.9	51.3	n.a.	n.a.	437.8	1197.2	4.48	58.5	−0.8 (5)	398.5	−26.3 (4)
900	171.9	21.8	n.a.	n.a.	151.2	385.2	4.52	29.7	11.2 (5)	439.5	−22.7 (3)
1000	25.3	7.1	n.a.	n.a.	210.2	467.1	4.52	98.0	−2.7 (5)	757.8	−21.4 (4)
1100	2.5	3.1	n.a.	n.a.	178.7	358.7	4.55	101.2	−0.4 (5)	352.4	−17.3 (4)
1200	57.2	5.0	n.a.	n.a.	33.9	b.d.	n.a.	46.7	2.2 (5)	205.6	−25.4 (3)
1300	b.d.	5.4	n.a.	n.a.	2.0	2.1	n.a.	1.8	−2.7 (5)	30.5	−27.3 (4)
1400	5.82	b.d.	n.a.	n.a.	b.d.	67.4	n.a.	0.2	−19.4 (1.1)	9.1	−25.6 (2)
Total	4474.1	809.1	11.60 (18)	0.0369 (32)	1381.2	3705.8	4.53	442.3	0.6 (5)	5658.9	−22.5 (3)

5–10% uncertainty in absolute concentrations of noble gases.
Numbers in parentheses refer to the last digits and are 1σ-uncertainties.
Uncertainties for $^{36}Ar/^{38}Ar$ are 0.01.
b.d. = below detection limit; n.a. = not analyzed.
[a] $\times 10^{-8}$ cm^3 STP g^{-1}.
[b] ppm.
[c] ‰

that later merged into the breccia). According to the Eugster et al. (2001) curve, irradiation should have happened much later than 1.8 Ga ago, when $(^{40}Ar/^{36}Ar)_{trapped}$ was about 2.5. This means that the soil was covered or shielded between 4.1 Ga and 1.8 Ga and was excavated and exposed 1.8 Ga ago for about 100–200 Ma. Subsequent thermal processes caused breccia formation, that is, agglutination to seal grain boundaries, and caused partial loss/fractionation of solar wind noble gases and transfer of them into vesicles. However, all that must not have reset the K-Ar system (otherwise, a 4.1 Ga plateau age could not be

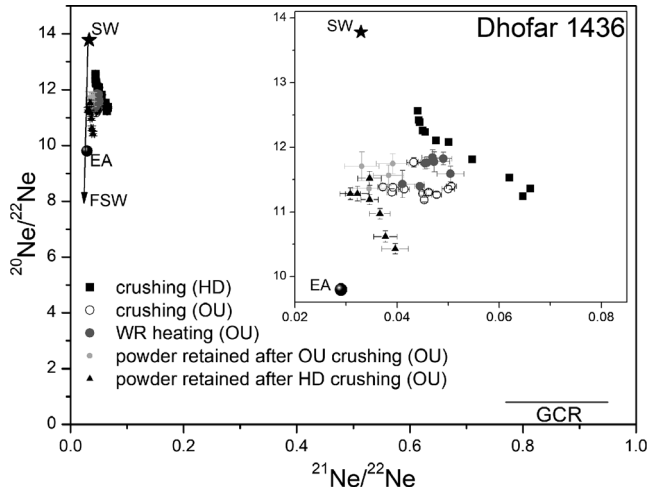

Fig. 7. Neon isotopic compositions for crushing and combustion analyses of Dhofar 1436. Solar wind (SW; Heber et al. 2009) and Earth's atmosphere (EA; Eberhardt et al. 1965) compositions are noted. The range for the cosmogenic component produced by galactic cosmic rays (GCR) is given: $(^{20}Ne/^{22}Ne)_c$ from Eugster and Michel (1995), $(^{21}Ne/^{22}Ne)_c$ using Leya et al. (2001) for 2π irradiation and shielding depths of up to 540 g cm^{-2} for average composition of highland lunar meteorites (Demidova et al. 2007), and using Eugster and Michel (1995) for 4π irradiation and different shielding depths for achondrites. HD = Heidelberg; OU = The Open University.

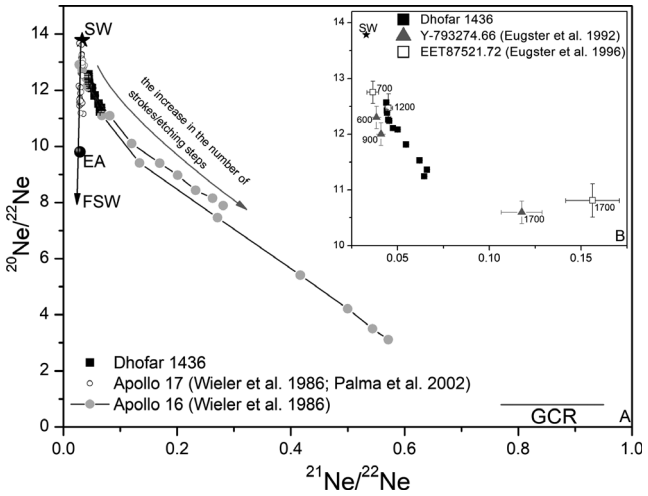

Fig. 8. Three-isotope plot of $^{20}Ne/^{22}Ne$ versus $^{21}Ne/^{22}Ne$ for lunar samples. A) Comparison of Ne measured in Dhofar 1436 by stepwise crushing performed in HD with Apollo soils analyzed by stepwise heating extraction. The data of Apollo 17 samples (71501 ilmenite and pyroxene measured by stepwise heating by Palma et al. [2002] and by etching by Wieler et al. [1986], respectively) show a linear array from SW Ne to fractionated solar wind (FSW) of heavier composition with increasing crushing steps. This trend is identical to modeled Ne isotopic profiles using the SRIM code (Grimberg et al. 2006) demonstrating the fractionation of SW Ne with depth (black arrow). The Apollo 16 data (64424 and 65511 plagioclase investigated by stepwise etching by Wieler et al. [1986] plot along curved lines that can be explained by mixing of fractionated SW-Ne and GCR-Ne (Grimberg et al. 2006). The Dhofar 1436 crushing data points display a similar pattern. In both Apollo 16 and Dhofar 1436, advanced crushing steps display the lowest SW/FSW-Ne component and the highest contribution of the GCR-Ne component. B) A similar release pattern can be observed for stepwise heating data of other lunar meteorites. Temperature steps in (°C) are labeled for Y-793274 and EET87521. Other components plotted include solar wind (SW; Heber et al. 2009) and Earth's atmosphere (EA; Eberhardt et al. 1965). The range for the cosmogenic component produced by galactic cosmic rays (GCR) is given: $(^{20}Ne/^{22}Ne)_c$ from Eugster and Michel (1995), $(^{21}Ne/^{22}Ne)_c$ using Leya et al. (2001) for 2π irradiation and shielding depths of up to 540 g cm^{-2} for average composition of highland lunar meteorites (Demidova et al. 2007) and using Eugster and Michel (1995) for 4π irradiation and different shielding depth for achondrites.

observed). This is particularly problematic, as part of the breccia is former melt, containing numerous bubbles, which—according to previous experiences with impact metamorphism and K-Ar dating—should have been reset completely. Moreover, before solidification and agglutination (i.e., between 4.1 Ga and 1.8 Ga), only 4.1 Ga old components were mixed into the breccia (e.g., like different lithic fragments and matrix in Dhofar 1436-a and Dhofar 1436-b). Specifically, during shielded storage and subsequent excavation and irradiation of the soil, neither older nor younger fragments must have been admixed to the yet not solidified soil.

We argue that the latter scenario requires some very unlikely or even impossible ad hoc assumptions, for example, (1) at 4.1 Ga, a complete reset of the K-Ar system without soil solidification; (2) keeping a loosely agglomerated soil package isolated for 2.3 Ga during burying, excavation, and surface irradiation; (3) during solidification, no partial loss of radiogenic ^{40}Ar. Particularly problematic is the question: how can one thermal process reset the soil at 4.1 Ga but without breccia solidification, while another thermal process (at 1.8 Ga) leaves the K-Ar system largely unaffected but causes breccia formation? From the viewpoint of resetting the K-Ar system, the 4.1 Ga event should have been stronger; from the viewpoint of breccia formation, the 1.8 Ga event should have been stronger—this is an unresolvable contradiction.

While the above arguments would strongly favor breccia formation 4.1 Ga ago and trapped surface correlated argon that accumulated before 4.1 Ga, its isotopic composition is incompatible with the Eugster et al. (2001) antiquity curve, again leading to a strong contradiction. There are other lunar meteorite Ar-Ar

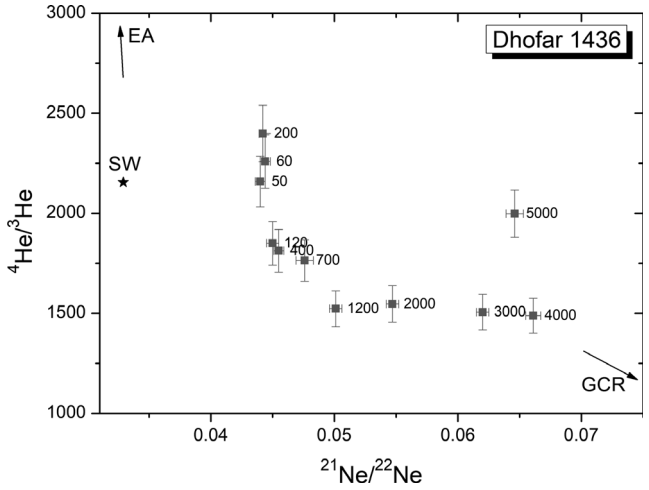

Fig. 9. ^{4}He/^{3}He versus ^{21}Ne/^{22}Ne for Dhofar 1436 crushing data obtained in HD. Solar wind (SW; Heber et al. 2009), Earth's atmosphere (EA; He: Mamyrin et al. 1970, Ne: Eberhardt et al. 1965), and the cosmogenic component produced by galactic cosmic ray (GCR; He: Reimer et al. [1998], Wieler [2002], Ne: calculated using Leya et al. [2001] for 2π irradiation and shielding depths of up to 540 g cm^{-2} for average composition of highland lunar meteorites [Demidova et al. 2007] and using Eugster and Michel [1995] for 4π irradiation and different shielding depths for achondrites) compositions are noted.

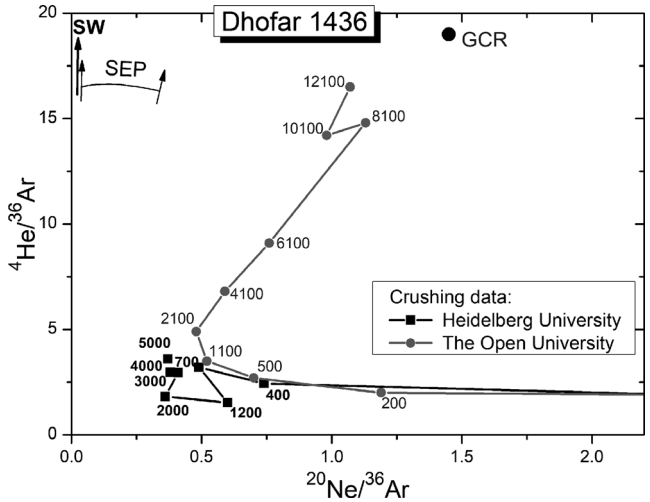

Fig. 10. Elemental abundance plot of ^{4}He/^{36}Ar versus ^{20}Ne/^{36}Ar ratios for Dhofar 1436 crushing data. Other components plotted include solar wind (SW; Heber et al. 2009), fractionated solar wind (SEP; Benkert et al. 1993: range based on step 16 of ilmenite 79035/3 and step 13 of pyroxene 71501/1), and cosmogenic component produced by galactic cosmic rays (GCR; Leya and Masarik 2009: average value for 0–150 cm radius using the chemical composition of Dhofar 1436).

data with ages and $(^{40}Ar/^{36}Ar)_{trapped}$ ratios that are either below or above the curve (Fernandes et al. 2000, 2003; Cohen et al. 2005b; Korochantseva et al. 2016), so there appears to be a general problem about the meaning and the interpretation of the orphan argon composition.

However, these contradictions may be resolved: If both high energetic (30 keV) ^{36}Ar and low energetic ^{40}Ar (1 keV) were implanted by solar wind, and if solar

Table 7. Elemental ratios of cosmogenic ^{3}He, ^{21}Ne, and ^{38}Ar released by stepwise crushing and WR combustion in Dhofar 1436 compared to model values.

Crushing, University of Heidelberg				Crushing, The Open University		WR heating		Galactic cosmic rays		
Extractions[a]	^{3}He/^{21}Ne	^{3}He/^{38}Ar	^{21}Ne/^{38}Ar	Extractions[a]	^{21}Ne/^{38}Ar	T (°C)	^{21}Ne/^{38}Ar	^{3}He/^{21}Ne	^{3}He/^{38}Ar	^{21}Ne/^{38}Ar
50				10	1.223	700	2.167	3.5–8.9[b]	7.8[b]	0.8–2.3[b]
60			3.343	50	0.578	800	2.873	2.4–3.3[c]	1.9–3.2[c]	0.8–1.0[c]
120	0.055	0.096	1.757	200	0.509	900	1.365			0.5–1.1[d]
200			0.736	500	0,358	1000	1,591			
400	0.272	0.112	0.413	1100	0.313	1100	1.386			
700	0.536	0.123	0.228	2100	0.280	1200	0.117			
1200	0.331	0.040	0.120	4100	0.187	1300	0.013			
2000	0.480	0.438	0.913	6100	0.152					
3000	0.558	0.310	0.556	8100	0.108					
4000	0.532	0.146	0.275	10100	0.146					
5000	0.123	0.020	0.162	12100	0.067					

The cosmogenic ratios in samples are evaluated using $(^3He/^4He)_{SW} = 4.64 \times 10^{-4}$ and $(^{21}Ne/^{22}Ne)_{sw} = 0.0329$ by Heber et al. (2009), $(^3He/^4He)_{cos} = 0.12$ by Wieler (2002), $(^{21}Ne/^{22}Ne)_{cos} = 0.86$ (average value for the $(^{21}Ne/^{22}Ne)_{cos}$ range, see Fig. 8), $(^{36}Ar/^{38}Ar)_{SW} = 5.47$ (Heber et al. 2009) and $(^{36}Ar/^{38}Ar)_{cos} = 0.65$ by Eugster et al. (1991).

[a]Cumulative number of strokes.

[b]Calculated using Eugster and Michel (1995) for 4π irradiation and different shielding depth for achondrites

[c]Calculated using Leya and Masarik (2009) for 4π irradiation of meteoroid with a radius of 150 g cm^{-2}.

[d]Calculated using Hohenberg et al. (1978) for 2π irradiation and shielding depth up to 500 g cm^{-2} for average. [b,c,d]calculated for average composition of lunar highland meteorites (Demidova et al. 2007).

heating before breccia formation 4.1 ago caused fractionation of solar wind He, Ne, and Ar (see below), such heating may well have resulted in lowering the $^{40}Ar/^{36}Ar$ ratio of trapped argon from about 12 down to 2.5, considering the very low implantation energy and easy thermal loss of ^{40}Ar when compared to ^{36}Ar (Baur et al. 1972).

Just as a sample calculation, the loss of a given isotope correlates with the inverse square of the diffusion distance according to the Carslaw and Jaeger (1959) equation:

$$F = 1 - 6\pi^{-2} \sum_{n=0}^{\infty} n^{-2} \exp\left(-n^2 \pi^2 Dt/a^2\right)$$

where F is the fractional loss, t diffusion time, a diffusion distance or grain radius, D diffusion coefficient with $D = D_0 \exp(-Q/RT)$, where Q is the activation energy, D_0 the frequency factor, R the gas constant, and T the temperature.

Assuming the same stopping power per keV for ^{40}Ar and ^{36}Ar, the diffusion distance for ^{40}Ar is 1/30 to that of ^{36}Ar. For a loss of 80% of ^{40}Ar, which is necessary to reduce $^{40}Ar/^{36}Ar$ from 12 to 2.5, we calculate (for $Dt/a^2 = 0.115$ for ^{40}Ar and $Dt/a^2 = 0.000128$ for ^{36}Ar) a 7% ^{36}Ar loss, which is feasible.

Hence, an irradiation scenario as a lunar soil before 4.1 Ga and subsequent heating (either prolonged solar and/or impact induced) may explain both the fractionation of solar wind noble gas (He, Ne, Ar) and the fractionation of orphan argon from $^{40}Ar/^{36}Ar$ of about 12 down to 2.5, followed by mixing with impact degassed material 4.1 Ga ago and breccia formation.

Noble Gas Elemental Ratios

In all analyses, the $^4He/^{20}Ne$, $^4He/^{36}Ar$, and $^{20}Ne/^{36}Ar$ ratios are strongly fractionated, that is, the light noble gases are depleted, relative to the heavy ones compared to the SW composition. Similar fractionation is observed for subsolar noble gases in enstatite chondrites (Okazaki et al. [2010], and references therein). The elemental abundances are also similar to other lunar samples (e.g., Wieler 2002; Schultz and Franke 2004). The mechanism for fractionation is considered to be diffusive loss of the light noble gases (Wieler 2016). Takaoka and Nakamura (1996) also detected trapped gases released by crushing experiments of an enstatite chondrite and the authors proposed that cosmogenic noble gases, radiogenic ^{40}Ar, and radiogenic ^{129}Xe accumulated prior to the shock event and became trapped and occluded in microbubbles upon impact melting. They also argued that additional mechanisms like solubility controlled degassing fractionation might play a role. It is likely that in Dhofar 1436, the 4.1 ± 0.1 Ga ago event having mobilized preexisting noble gas components (SW, radiogenic, and cosmogenic) caused the fractionation, resulting in significant loss of SW He and Ne.

It should be noted that only totals and stepwise crushing data reflect truly in situ elemental ratios, for example, $^4He/^{20}Ne$ and $^{20}Ne/^{36}Ar$. Stepwise heating data do not, as these can be affected by diffusional fractionation upon stepwise heating extraction. As light noble gases can be more easily extracted by thermally driven diffusion; this effect would be recognizable by too high $^4He/^{20}Ne$ and $^{20}Ne/^{36}Ar$ ratios in low temperature extractions which then gradually turn to anomalously low $^4He/^{20}Ne$ and $^{20}Ne/^{36}Ar$ ratios in high temperature extractions (Fig. 6). Hence, we will focus our considerations on totals and stepwise crushing data. Figure 10 shows that the $^4He/^{20}Ne$ and $^4He/^{36}Ar$ ratios observed during stepwise crushing extractions are clearly lower than in unfractionated solar wind and in the GCR produced cosmogenic component. Only upon prolonged crushing after >2000 strokes, the ratios show a trend toward a cosmogenic component (Fig. 10). This is consistent with the more cosmogenic character of the isotopic ratios ($^4He/^3He$, $^{21}Ne/^{22}Ne$) in advanced crushing steps.

Basically the elemental ratio variations in crushing steps can be explained by successive opening of voids/inclusions of different sizes. It should be noted that the significant increase of the $^4He/^{20}Ne$ and $^4He/^{36}Ar$ ratios cannot be explained solely by admixing of nucleogenic or cosmogenic ^4He. Another source of ^4He could be mechanical breakdown of the crystal structure releasing radiogenic ^4He, causing significant effects on the measured $^3He/^4He$ ratios during crushing experiments (Scarsi 2000; Matsumoto et al. 2002; Buikin et al. 2018). However, in Dhofar 1436, the $^3He/^4He$ ratio systematically increases with crushing steps, so there is no indication of the in situ radiogenic ^4He contribution in the advanced crushing steps, but rather an increasing contribution of cosmogenic ^3He (Fig. 9). A higher production rate of cosmogenic He compared to cosmogenic Ne and Ar (Leya and Masarik 2009) also cannot explain a factor of 10 increase of the $^4He/^{20}Ne$ and $^4He/^{36}Ar$ ratios during progressive crushing, since the contribution of cosmogenic ^4He to the ^4He budget is very low (see above). The increase of these ratios obviously reflects a truly different elemental ratio of the fractionated SW component between crush-accessible sites varying in size, for example, between larger and smaller voids. The increase of $^{20}Ne/^{36}Ar$ during progressive crushing is also observed but less pronounced compared to the He/Ne and He/Ar ratios and is demonstrated by more intensive crushing

performed at the OU (Fig. 10). The analogous increase of $^{4}He/^{20}Ne$ and $^{4}He/^{36}Ar$ ratios with progressive crushing is also reported for the L-chondrite Ghubara (Korochantseva et al. 2018) and it seems to be controlled by very similar processes.

The elemental ratios of cosmogenic ^{3}He, ^{21}Ne, and ^{38}Ar released by crushing are strongly fractionated compared to the production rate ratios of these isotopes calculated according to Hohenberg et al. (1978), Eugster and Michel (1995), and Leya and Masarik (2009) for the Dhofar 1436 chemical composition (Table 7). For example, $(^{3}He/^{38}Ar)_{cos}$ is mostly ≤ 0.1 compared to literature or model values of >1.9 (Table 7). Concerning $(^{21}Ne/^{38}Ar)_{cos}$ only, the first crushing steps are within the range of unfractionated values between 1 and 3, most advanced crushing step values are lower (Table 7) and accompanied by fractionated trapped gases (Fig. 10; Tables 2 and 3). As advanced crushing steps also show $^{40}Ar/^{36}Ar$ ratios in the range of the trapped argon composition defined by the intermediate to high temperature isochrones (Fig. 3), we may conclude that vesicle-related fractionated cosmogenic gases are associated with the high temperature components. Nevertheless, it should be noted that the fractionation of the solar wind component is stronger (a factor of about 80 for $^{20}Ne/^{36}Ar$ and at least 2000 for $^{4}He/^{36}Ar$) than for the cosmogenic noble gases (up to a factor of about 20 for $^{21}Ne/^{38}Ar$ and about 100 for $^{3}He/^{38}Ar$).

All in all, noble gas elemental ratios released during crushing can be interpreted by mixing of variable fractionated solar and cosmogenic components. The significant fractionation of the cosmogenic gases suggests that the main part of cosmogenic nuclides in Dhofar 1436 was accumulated early over a long time period (>150 Ma according to CRE age spectrum, Fig. 5C), was redistributed, and fractionated during the main impact event 4.1 ± 0.1 Ga ago and was finally trapped into voids. The fractionation of accumulated solar and cosmogenic noble gases could have happened before breccia formation of Dhofar 1436 caused by solar heating of the regolith. The amount of cosmogenic gases with unfractionated composition in tracks of late accumulation is obviously low. Later, "solar heating" or late mild impacts were likely not responsible for the main component of high temperature fractionated cosmogenic gases as temperature extractions $\leq$1100 °C do not show fractionation of cosmogenic gases.

Ne Curved Function

In the neon three-isotope diagram (Fig. 8), there is a remarkable coincidence of isotopic trends: the first extraction steps are dominated by solar wind composition, the following steps develop toward fractionated solar wind, and finally toward cosmogenic composition, regardless of whether neon is extracted by stepwise etching (Apollo samples; Wieler et al. 1986) or stepwise crushing (Dhofar 1436). The curvature of the neon trend of Dhofar 1436 obtained by crushing could be partially caused by the presence of two cosmogenic components, ancient fractionated (redistributed during the main event into voids) and recent, located in different sites.

Only a few stepwise crushing investigations of extraterrestrial material have been performed so far. Additional studies of meteorites using this technique would help in fully evaluating the type of observations made in this study.

Carbon and Nitrogen

The powdered samples contain excess N and C concentrations in comparison with the WR sample, similar to an observation made in a previous study (Verchovsky et al. 2017). This is most likely related to methodological artifacts: On the one hand, organic material and air components are trapped by fresh grain surfaces after exposing the crushed material to air and these components are released at low temperatures. On the other hand, the steel particles from the crusher, formed as a result of friction between its metal parts, introduce additional N and C that are both released at high temperatures. Therefore, N and C data for powdered samples will not be discussed; instead, we will focus on data of crushed and combusted WR samples.

The C concentration of the step-combusted WR sample (Dhofar 1436-e) is 555.3 ppm, with $\delta^{13}C$ of −28‰ to +11‰ (Table 4). Nitrogen concentrations released by crushing and WR combustion are 3.2 ppm and 20.8 ppm, respectively. The release pattern of nitrogen for Dhofar 1436, analyzed by stepwise combustion carried out at the OU, is bimodal (Fig. 11A). During crushing, most of the N is released during the initial steps. At the beginning of the crushing, $\delta^{15}N$ decreases from −12‰ to −36‰ and then increases up to + 4‰ (Table 3; Fig. 11B). In the initial crushing steps, the ^{15}N-enriched signature is likely related to atmospheric/organic contamination. For the final crushing steps, cosmogenic nitrogen contributes to the positive value. The latter is supported by the aforementioned trends for the noble gas isotopic composition. The lightest nitrogen composition ($\delta^{15}N = -79‰$) is in the range observed earlier for lunar samples (e.g., Brilliant et al. 1994; Assonov et al. 2002; Hashizume et al. 2002) and it is associated with SW nitrogen measured during stepwise combustion of the WR sample at the 1200 °C release peak (Fig. 11B).

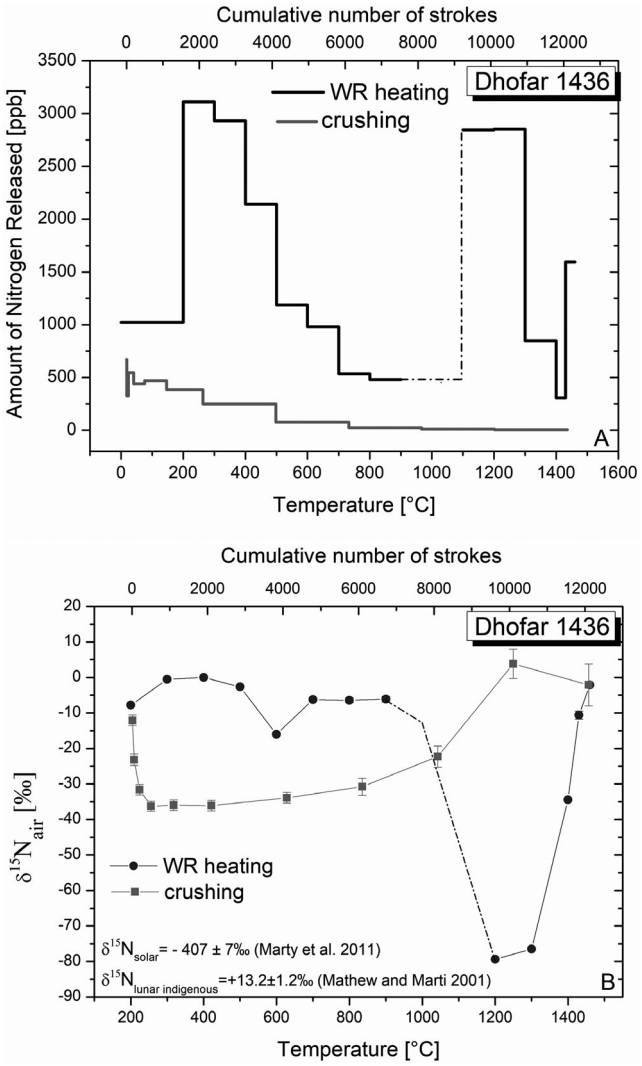

Fig. 11. Nitrogen abundances (A) and isotopic compositions (B) obtained by stepwise combustion and crushing analyses performed at the OU. The lightest nitrogen composition ($\delta^{15}N = -79‰$) is measured during stepwise heating of whole rock sample at the main release peak (1200 °C) of Ne and Ar (Ar-Ar data).

Note that also the majority of the Ne and Ar is released at this temperature. High temperature degassing of minerals is obviously the consequence of shock metamorphism (e.g., Trieloff et al. 2018). A small release peak of carbon is also observed at this temperature (Fig. 12), having the most ^{13}C-enriched signature (+11‰). This finding is likely related to oxidation of graphite. Similar release patterns of N and C and $\delta^{15}N$ and $\delta^{13}C$ variation have been observed for Dar al Gani 262 (Bischoff et al. 1998). In contrast to lunar soils, which show the presence of both isotopically heavy (up to +150‰ at relatively low temperature steps, of planetary origin accreting to the Moon) and light (down to −150‰ at higher temperature steps, of

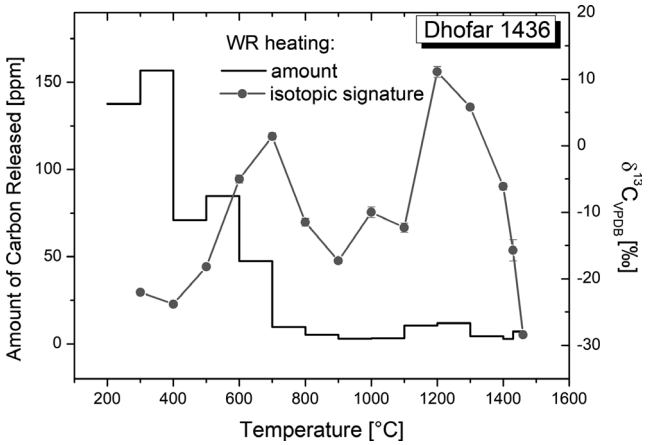

Fig. 12. Abundances and isotopic compositions of carbon analyzed by stepwise whole rock combustion.

solar origin) nitrogen components (Becker et al. 1976; Brilliant et al. 1994; Assonov et al. 2002; Mortimer et al. 2016), the lunar meteorites (Dhofar 1436 and DaG 262) exhibit only the isotopically light N component. Evidently the isotopic composition of nitrogen redistributed into voids during breccia formation is dominated by solar gases accumulated before the major event as we already discussed for the noble gas data. The low temperature heavy nitrogen could have been lost at the impact events.

In recent studies, the variations of $\delta^{15}N$ in lunar samples is considered to be due to temporal changes in the micrometeorite flux (e.g., Hashizume et al. 2002; Füri et al. 2012). Hence, a simple relation between age and $\delta^{15}N$ is not tenable as in the case of orphan argon (see the Lunar Trapped Argon and the "Antiquity" section). For the impact melt breccia Dhofar 1436, the lunar nitrogen isotopic composition is rather a result of mobilization of nitrogen components that accumulated prior to the 4.1 Ga event and redistribution within the rock as it is also suggested for noble gases.

SUMMARY

The K-Ar system of the gas-rich lunar impact melt breccia Dhofar 1436 was totally reset at 4.1 ± 0.1 Ga by an event potentially related to the purported LHB. Later, this meteorite may have experienced a thermal partial degassing event causing diffusional losses of argon recognized for cosmogenic isotopes. Dhofar 1436 has a complex cosmic ray exposure history. The main part of the cosmogenic nuclides in Dhofar 1436 was likely accumulated before the 4.1 ± 0.1 Ga event over an extended period of time (>150 Ma); the amount of cosmogenic gases from the late and second accumulation phase is obviously low. The transit time

of the meteorite from the lunar surface to Earth and recent exposure on the lunar surface is <14 Ma.

A combined stepwise crushing and combustion study of noble gases and nitrogen in this breccia as well as Ar-Ar dating showed that these volatiles are released at high temperatures and that they have been trapped in voids. The origin of the volatile species, and, in particular, the lunar trapped argon with $^{40}Ar/^{36}Ar$ ratios of 2–3 identified in all analyzed samples, and inter alia, precisely determined by Ar-Ar isochron evaluations, giving $^{40}Ar/^{36}Ar = 2.51 \pm 0.04$, are linked with a major breccia forming event. This event likely comprised grain compression and agglutination at partially open porosity conditions, allowing gases from grain boundaries to escape partially and to fractionate. It also comprised closed porosity conditions, caused by sintering and sealing of grain boundaries. Former grain boundaries encapsulate partly vesicular/porous interiors of the compacted breccia, in which former surface correlated noble gases become trapped. This process explains the strong retention of solar wind isotopes in vesicles throughout the interior of the breccia and their strong fractionation upon extraction by stepwise crushing.

Isotopic and elemental compositions of the light noble gases released by crushing can be explained as a mixture of solar-like and cosmogenic (ancient and recent) components. The isotopic compositions of trapped He and Ne are dominated by the SW component: In the first crushing steps, $^{4}He/^{3}He$ ratios correspond to the solar wind value and $^{20}Ne/^{22}Ne$ ratios are up to 12.57. The higher contribution of the cosmogenic component is observed in advanced crushing steps. This is also valid for Ar and N isotopic compositions as well as noble gas elemental ratios. The solar and cosmogenic components were strongly fractionated; fractionation of the solar wind component is stronger than for cosmogenic noble gases. The increase of the $^{4}He/^{20}Ne$, $^{4}He/^{36}Ar$, and $^{20}Ne/^{36}Ar$ elemental ratios upon progressive crushing likely point out disequilibrium distribution of the gases between the voids of different sizes that can be caused by the dynamics of the shock metamorphism process.

The lightest nitrogen composition ($\delta^{15}N = -79‰$) associated with the most ^{13}C-enriched signature (+11‰) is observed during stepwise combustion of the WR sample at 1200 °C, which is also the main degassing peak of Ne and Ar and which is likely due to release from voids of shock metamorphic phases. This also demonstrates that a nitrogen component related to micrometeorite contamination of the lunar surface (Assonov et al. 2002; Mortimer et al. 2016) can be transferred into highly retentive shock phases (including vesicles) together with other former surface related solar wind implanted noble gases, resulting in almost identical release patterns despite their different origin and different chemical properties.

We consider two alternative formation models to explain our observations. In Model 1, breccia formation and shock metamorphism occurred during the LHB at 4.1 Ga ago, followed by impact-induced mobilization, equilibration, fractionation, and re-trapping of pre-existing solar wind, planetary, cosmogenic gases, radiogenic, and reimplanted argon by agglutination of former grain boundaries leading to vesicle formation and sealing. Hence, gases are related to voids of retentive phases formed during shock metamorphism, and can be released by crushing or thermal degassing at high temperatures. Later, unfractionated cosmogenic nuclides were acquired for a few tens of Ma, before the rather recent ejection event from the Moon.

In Model 2, complete reset occurred 4.1 Ga ago. However, the reset was primarily induced thermally (e.g., long-term tempering by an impact melt sheet), and was not necessarily accompanied by formation of shock phases or breccia formation. The soil was only loosely agglomerated, to enable later acquisition of cosmogenic gases together with solar wind and orphan argon by ion implantation. This irradiation should have happened 1.8 Ga ago, when $(^{40}Ar/^{36}Ar)_{trapped}$ was about 2.5 (Eugster et al. 2001). This means that the soil was covered or shielded between 4.1 Ga and 1.8 Ga and was excavated and exposed 1.8 Ga ago for about 100–200 Ma of irradiation. Fractionation of solar wind and cosmogenic nuclides was induced by solar heating of the soil during exposure. An impact event a few tens of Ma ago led to the formation of shock phases (highly retentive) but caused only minor loss of noble gases. Finally, unfractionated cosmogenic nuclides were acquired for a few tens of Ma just before the rather recent ejection event.

Major problems with Model 2 are that late breccia formation requires formation from constituents of very similar (4.1 Ga) age, that is, for a very long time during shielded storage and subsequent excavation and irradiation of the soil (4.1–1.8 Ga ago), neither older nor younger fragments were admixed to the yet not solidified soil. Another unresolvable contradiction is the question of how can the 4.1 Ga event have reset the K-Ar system, but have avoided breccia formation, while the later breccia-forming event leaves the K-Ar system nearly unaffected? Finally, the breccia Dhofar 1436 consists of clasts (of which lithic fragments are mainly impact melt breccias), which are cemented by a partly devitrified glassy matrix with numerous bubbles. It is likely that the clasts were heated by melt within both matrix and clasts resulting in total loss of radiogenic ^{40}Ar. In particular, the melt glass portion should be

reset during a breccia-forming event, so rather the 4.1 Ga age should correspond to the breccia formation time. If the breccia solidified 4.1 Ga ago, the later acquisition of solar wind and orphan gases by implantation could not have been effective, because acquisition of high solar wind abundances requires intense regolith gardening and exposure of individual grains. In view of these issues, we consider the first scenario of breccia formation as more plausible; however, this is in contradiction with the evolution curve of $(^{40}Ar/^{36}Ar)_{trapped}$ in the antiquity model (Eugster et al. 2001). As a tentative explanation, we suggest substantial fractionation of highly energetic implanted (30 keV) ^{36}Ar and shallowly implanted ^{40}Ar (1 keV), which could occur by thermal disturbance before breccia formation, when original implantation sites are relevant for diffusion processes. A calculation shows that an $^{40}Ar/^{36}Ar$ ratio of trapped orphan argon from approximately 12 down to 2.5 is feasible, considering the very low implantation energy and easy thermal loss of ^{40}Ar when compared to ^{36}Ar. However, a more detailed consideration of this process should be envisaged by future studies.

Acknowledgments—We thank reviewers Ingo Leya, Timothy Swindle, Rainer Wieler, and Ryuji Okazaki for helpful criticism and suggestions that improved the quality of this manuscript, as well as editor in chief A. J. Timothy Jull for thorough and constructive handling of this article. The authors acknowledge support by Klaus Tschira Stiftung GmbH. M.A. would like to acknowledge funding from the UK Science and Technology Facilities Council (grant# ST/L000776/1 and grant# ST/P000657/1), and the UK Space Agency (grant# ST/R001391/1). This study is a contribution to research theme no. 0137-2019-0015 (Vernadsky Institute).

Editorial Handling—Prof. Ingo Leya

REFERENCES

Assonov S. S., Franchi I. A., Pillinger C. T., Semenova A. S., Shukolyukov Y. A., Verchovsky A. B., and Iassevitch A. N. 2002. Nitrogen and argon release profiles in Luna 16 and Luna 24 regolith samples: The effects of regolith reworking. *Meteoritics & Planetary Science* 37:27–48.

Baur H., Frick U., Funk H., Schultz L., and Signer P. 1972. Thermal release of helium, neon, and argon from lunar fines and minerals. Proceedings, 3rd Lunar Science Conference. pp. 1947–1966.

Becker R. H. and Clayton R. N. 1975. Nitrogen abundances and isotopic compositions in lunar samples. Proceedings, 6th Lunar Science Conference. pp. 2131–2149.

Becker R. H., Clayton R. N., and Mayeda T. K. 1976. Characterization of lunar nitrogen components. Proceedings, 7th Lunar Science Conference. pp. 441–458.

Bekaert D. V., Avice G., Marty B., Gudipati M. S., and Henderson B. L. 2015. Searching for indigenous noble gases in the Moon: Vacuum crushing of vesicular basalt 15016 and stepwise heating of anorthosites 60025, 60215 and 65315 aliquots (abstract). American Geophysical Union. id.P11A-2063.

Bekaert D. V., Avice G., and Marty B. 2018. Origin and significance of cosmogenic signatures in vesicles of lunar basalt 15016. *Meteoritics & Planetary Science* 53:1238–1251.

Benkert J.-P., Baur H., Signer P., and Wieler R. 1993. He, Ne, and Ar from the solar wind and solar energetic particles in lunar ilmenites and pyroxenes. *Journal of Geophysical Research* 98:13,147–13,162.

Bernatowicz T. J., Hohenberg C. M., Hudson B., Kennedy B. M., Laul J. C., and Podosek F. A. 1980. Noble gas component organization in 14301. Proceedings, 11th Lunar and Planetary Science Conference. pp. 629–668.

Bischoff A., Weber D., Clayton R. N., Faestermann T., Franchi I. A., Herpers U., Knie K., Korschinek G., Kubik P. W., Mayeda T. K., Merchel S., Michel R., Neumann S., Palme H., Pillinger C. T., Schultz L., Sexton A. S., Spettel B., Verchovsky A. B., Weber H. W., Weckwerth G., and Wolf D. 1998. Petrology, chemistry, and isotopic compositions of the lunar highland regolith breccia Dar al Gani 262. *Meteoritics & Planetary Science* 33:1243–1257.

Bogard D. D. and Hirsch W. C. 1980. ^{39}Ar-^{40}Ar dating, Ar diffusion properties, and cooling rate determinations of severely shocked chondrites. *Geochimica et Cosmochimica Acta* 44:1667–1682.

Bogard D. D., Nyquist L. E., Bansal B. M., Wiesmann H., and Shih C. Y. 1975. 76535: An old lunar rock. *Earth and Planetary Science Letters* 26:69–80.

Brereton N. R. 1970. Corrections for interfering isotopes in the $^{40}Ar/^{39}Ar$ dating method. *Earth and Planetary Science Letters* 8:427–433.

Brilliant D. R., Franchi I. A., and Pillinger C. T. 1994. Nitrogen components in lunar soil 12023: Complex grains are not the carrier of isotopically light nitrogen. *Meteoritics & Planetary Science* 29:718–723.

Buikin A. I., Trieloff M., Hopp J., Althaus T., Korochantseva E. V., Schwarz W., and Altherr R. 2005. Noble gas isotopes suggest deep mantle plume source of late Cenozoic mafic alkaline volcanism in Europe. *Earth and Planetary Science Letters* 230:143–162.

Buikin A. I., Verchovsky A. B., Lorenz C. A., Skripnik A. Y., and Korochantseva E. V. 2013. Noble gases and nitrogen released by crushing from Pesyanoe aubrite (abstract #1141). 44th Lunar and Planetary Science Conference. CD-ROM.

Buikin A. I., Solovova I. P., Verchovsky A. B., Kogarko L. N., and Averin A. A. 2014. PVT parameters of fluid inclusions and the C, O, N, and Ar isotopic composition in a garnet lherzolite xenolith from the Oasis Jetty, East Antarctica. *Geochemistry International* 52:805–821.

Buikin A. I., Hopp J., Lorenz C. A., and Trieloff M. 2015. Noble gas isotope composition and elemental ratios in Pesyanoe aubrite: Stepwise crushing data (abstract). 78th Annual Meeting of the Meteoritical Society. *Meteoritics & Planetary Science* 50:5110.

Buikin A. I., Kamaleeva A. I., and Sorohtina N. V. 2018. On the separation efficiency of entrapped and in situ noble gas components at sample crushing in vacuum. *Geochemistry International* 56:601–608.

Carslaw H. S. and Jaeger J. C. 1959. *Conduction of heat in solids*, 2nd ed. Oxford, UK: Oxford University Press. 310 p.

Cohen B. A., Swindle T. D., Taylor L. A., and Nazarov M. A. 2002. ^{40}Ar-^{39}Ar ages from impact melt clasts in lunar meteorites Dhofar 025 and Dhofar 026 (abstract #1252). 33rd Lunar and Planetary Science Conference. CD-ROM.

Cohen B. A., Swindle T. D., and Kring D. A. 2005a. Geochemistry and ^{40}Ar-^{39}Ar geochronology of impact-melt clasts in feldspathic lunar meteorites: Implications for lunar bombardment history. *Meteoritics & Planetary Science* 40:755–777.

Cohen B. A., Swindle T. D., Kring D. A., and Olson E. K. 2005b. Geochemistry and ^{40}Ar-^{39}Ar geochronology of impact-melt clasts in lunar meteorites Dar al Gani 262 and Calcalong Creek (abstract #1481). 36th Lunar and Planetary Science Conference. CD-ROM.

Connolly H. C. Jr., Smith C., Benedix G., Folco L., Righter K., Zipfel J., Yamaguchi A., and Chennaoui Aoudjehane H. 2008. The Meteoritical Bulletin, No. 93. *Meteoritics & Planetary Science* 43:571–632.

Demidova S. I., Nazarov M. A., Lorenz C. A., Kurat G., Brandstätter F., and Ntaflos T. 2007. Chemical composition of lunar meteorites and the lunar crust. *Petrology* 15:386–407.

Eberhardt P., Eugster O., and Marti K. 1965. A redetermination of the isotopic composition of atmospheric neon. *Zeitschrift Naturforschung Teil A* 20:623–624.

Eugster O. and Michel T. 1995. Common asteroid break-up events of eucrites, diogenites, and howardites and cosmic-ray production rates for noble gases in achondrites. *Geochimica et Cosmochimica Acta* 59:177–199.

Eugster O., Beer J., Burger M., Finkel R. C., Hofmann H. J., Krähenbühl U., Michel T., Synal H. A., and Wölfli W. 1991. History of the paired lunar meteorites MAC88104 and MAC88105 derived from noble gas isotopes, radionuclides, and some chemical abundances. *Geochimica et Cosmochimica Acta* 55:3139–3148.

Eugster O., Michel T., and Niedermann S. 1992. Solar wind and cosmic ray exposure history of lunar meteorite Yamato-793274. *Proceedings of the National Institute for Polar Research Symposium on Antarctic Meteorites* 5:23–35.

Eugster O., Thalmann C., Albrecht A., Herzog G. F., Delaney J. S., Klein J., and Middleton R. 1996. Exposure history of glass and breccia phases of lunar meteorite EET87521. *Meteoritics & Planetary Science* 31:299–304.

Eugster O., Terribilini D., Polnau E., and Kramers J. 2001. The antiquity indicator argon-40/argon-36 for lunar surface samples calibrated by uranium-235-xenon-136 dating. *Meteoritics & Planetary Science* 36:1097–1115.

Fagan A. L., Joy K. H., Bogard D. D., and Kring D. A. 2014. Ages of globally distributed lunar paleoregoliths and soils from 3.9 Ga to the present. *Earth, Moon, and Planets* 112:59–71.

Fernandes V. A., Burgess R., and Turner G. 2000. Laser argon-40-argon-39 age studies of Dar al Gani 262 lunar meteorite. *Meteoritics & Planetary Science* 35:1355–1364.

Fernandes V. A., Burgess R., and Turner G. 2003. ^{40}Ar-^{39}Ar chronology of lunar meteorites Northwest Africa 032 and 773. *Meteoritics & Planetary Science* 38:555–564.

Fernandes V. A., Anand M., Burgess R., and Taylor L. A. 2004. Ar-Ar studies of Dhofar clast-rich feldspathic highland meteorites: 025, 026, 280, 303 (abstract #1514). 35th Lunar and Planetary Science Conference. CD-ROM.

Friedman I., O'Neil J. R., Adami L. H., Gleason J. D., and Hardcastle K. 1970. Water, hydrogen, deuterium, carbon, carbon-13, and oxygen-18 content of selected lunar material. *Science* 167:538–540.

Fukuda D., Nakmura T., Takaoka N., and Nagao K. 1996. Noble gas analysis of the Julesburg L3.6, Tulia H4, Y-86789 thermally metamorphosed CM, and Allende CV3 chondrites by crushing method (abstract). 27th Lunar and Planetary Science Conference. p. 385.

Funkhouser J., Jessberger E., Müller O., and Zähringer J. 1971. Active and inert gases in Apollo 12 and Apollo 11 samples released by crushing at room temperature and by heating at low temperatures. Proceedings, 2nd Lunar Science Conference. pp. 1381–1396.

Füri E., Marty B., and Assonov S. S. 2012. Constraints on the flux of meteoritic and cometary water on the Moon from volatile element (N-Ar) analyses of single lunar soil grains, Luna 24 core. *Icarus* 218:220–229.

Geiss J. and Bochsler P. 1982. Nitrogen isotopes in the solar system. *Geochimica et Cosmochimica Acta* 46:529–548.

Gibson E. K. Jr. and Andrawes F. F. 1978. Nature of the gases release from lunar rocks and soils upon crushing. Proceedings, 9th Lunar and Planetary Science Conference. pp. 2433–2450.

Gibson E. K. Jr., Graham D. G., and Andrawes F. F. 1979. Inorganic gases released upon crushing and pyrolysis of chondritic meteorites. *Meteoritics* 14:402.

Göbel R., Ott U., and Begemann F. 1978. On trapped noble gases in ureilites. *Journal of Geophysical Research* 83:855–867.

Grimberg A., Baur H., Bochsler P., Bühler F., Burnett D. S., Hays C. C., Heber V. S., Jurewicz A. J. G., and Wieler R. 2006. Solar wind neon from Genesis: Implications for the lunar noble gas record. *Science* 314:1133–1135.

Hashizume K., Marty B., and Wieler R. 2002. Analyses of nitrogen and argon in single lunar grains: Towards a quantification of the asteroidal contribution to planetary surfaces. *Earth and Planetary Science Letters* 202:201–216.

Heber V. S., Wieler R., Baur H., Olinger C., Friedmann T. A., and Burnett D. S. 2009. Noble gas composition of the solar wind as collected by the Genesis mission. *Geochimica et Cosmochimica Acta* 73:7414–7432.

Heymann D. and Kirsten T. 1973. Argon systematics in lunar fines (abstract). 4th Lunar and Planetary Science Conference. p. 362.

Heymann D., Yaniv A., Adams J. A. S., and Fryer G. E. 1970. Inert gases in lunar samples. *Science* 167:555–558.

Heymann D., Walton J. R., Jordan J. L., Lakatos S., and Yaniv A. 1974. Light and dark soils at the Apollo 16 landing site. *The Moon* 13:81–110.

Heymann D. and Yaniv A. 1970. Ar^{40} anomaly in lunar samples from Apollo 11. Proceedings of the Apollo 11 Lunar Science Conference. pp. 1261–1267.

Heymann D. and Yaniv A. 1971. Breccia 10065: Release of inert gases by vacuum crushing at room temperature.

Proceedings, 2nd Lunar Science Conference. pp. 1681–1692.
Hilton D. R., Hammerschmidt K., Teufel S., and Friedrichsen H. 1993. Helium isotope characteristics of Andean geothermal fluids and lavas. *Earth and Planetary Science Letters* 120:265–282.
Hohenberg C. M., Davis P. K., Kaiser W. A., Lewis R. S., and Reynolds J. H. 1970. Trapped and cosmogenic rare gases from stepwise heating of Apollo 11 samples. Proceedings, 11th Lunar and Planetary Science Conference. pp. 1283–1309.
Hohenberg C. M., Marti K., Podosek F. A., Reedy R. C., and Shirck J. R. 1978. Comparisons between observed and predicted cosmogenic noble gases in lunar samples. Proceedings, 9th Lunar and Planetary Science Conference. pp. 2311–2344.
Hopp J., Trieloff M., Buikin A. I., Korochantseva E. V., Schwarz W. H., Althaus T., and Altherr R. 2007. Heterogeneous mantle argon isotope composition in the subcontinental lithospheric mantle beneath the Red Sea region. *Chemical Geology* 240:36–53.
Huneke J. C., Podosek F. A., and Wasserburg G. J. 1973. An argon bouillabaisse including ages from the Luna 20 site (abstract). 4th Lunar Science Conference. p. 403.
Jessberger E. K., Dominik B., Staudacher T., and Herzog G. F. 1980. ^{40}Ar-^{39}Ar ages of Allende. *Icarus* 42:380–405.
Joy K. H., Kring D. A., Bogard D. D., McKay D. S., and Zolensky M. E. 2011. Re-examination of the formation ages of the Apollo 16 regolith breccias. *Geochimica et Cosmochimica Acta* 75:7208–7225.
Kerridge J. F. 1975. Solar nitrogen: Evidence for a secular increase in the ratio of nitrogen-15 to nitrogen-14. *Science* 188:162–164.
Kerridge J. F. 1989. What has caused the secular increase in solar nitrogen-15? *Science* 245:480–486.
Koike M., Sumino H., Sano Y., and Ozima M. 2017. Combined stepwise heating and vacuum crushing analyses of noble gases in shergottites (abstract #1866). 48th Lunar and Planetary Science Conference. CD-ROM.
Korochantseva E. V., Trieloff M., Lorenz C. A., Buykin A. I., Ivanova M. A., Schwarz W. H., Hopp J., and Jessberger E. K. 2007. L-chondrite asteroid breakup tied to Ordovician meteorite shower by multiple isochron ^{40}Ar-^{39}Ar dating. *Meteoritics & Planetary Science* 42:113–130.
Korochantseva E. V., Trieloff M., Buikin A. I., and Hopp J. 2009. Shergottites Dhofar 019, SaU 005, Shergotty, and Zagami: ^{40}Ar-^{39}Ar chronology and trapped Martian atmospheric and interior argon. *Meteoritics & Planetary Science* 44:293–321.
Korochantseva E. V., Buikin A. I., Hopp J., Lorenz C. A., Korochantsev A. V., Ott U., and Trieloff M. 2016. Thermal and irradiation history of lunar meteorite Dhofar 280. *Meteoritics & Planetary Science* 51:2334–2346.
Korochantseva E. V., Buikin A. I., and Trieloff M. 2017. Trapped extraterrestrial argon in meteorites. *Geochemistry International* 55:971–976.
Korochantseva E. V., Buikin A. I., Verchovsky A. B., Lorenz C. A., and Korochantsev A. V. 2018. Noble gases, nitrogen and carbon isotopic compositions of the Ghubara meteorite, revealed by stepwise combustion and crushing methods. *Geochemistry International* 56:1384–1397.
Kunz J., Falter M., and Jessberger E. K. 1997. Shocked meteorites: Argon-40-argon-39 evidence for multiple impacts. *Meteoritics & Planetary Science* 32:647–670.
Lee J.-Y., Marti K., Severinghaus J. P., Kawamura K., Yoo H.-S., Lee J. B., and Kim J. S. 2006. A redetermination of the isotopic abundances of atmospheric Ar. *Geochimica et Cosmochimica Acta* 70:4507–4512.
Leya I. and Masarik J. 2009. Cosmogenic nuclides in stony meteorites revisited. *Meteoritics & Planetary Science* 44:1061–1086.
Leya I., Neumann S., Wieler R., and Michel R. 2001. The production of cosmogenic nuclides by galactic cosmic-ray particles for 2π exposure geometries. *Meteoritics & Planetary Science* 36:1547–1561.
Mamyrin B. A., Anufriyev G. S., Kamenskii I. L., and Tolstikhin I. N. 1970. Determination of the isotopic composition of atmospheric helium. *Geochemistry International* 7:498–505.
Manka R. H. and Michel F. C. 1971. Lunar atmosphere as a source of lunar surface elements. Proceedings, 2nd Lunar Science Conference. pp. 1717–1728.
Marty B., Zimmermann L., Burnard P. G., Wieler R., Heber V. S., Burnett D. L., Wiens R. C., and Bochsler P. 2010. Nitrogen isotopes in the recent solar wind from the analysis of Genesis targets: Evidence for large scale isotope heterogeneity in the early solar system. *Geochimica et Cosmochimica Acta* 74:340–355.
Marty B., Chaussidon M., Wiens R. C., Jurewicz A. J. G., and Burnett D. S. 2011. A ^{15}N-poor isotopic composition for the solar system as shown by Genesis solar wind samples. *Science* 332:1533–1536.
Mathew K. J. and Marti K. 2001. Lunar nitrogen: Indigenous signature and cosmic-ray production rate. *Earth and Planetary Science Letters* 184:659–669.
Matsumoto T., Seta A., Matsuda J., Takebe M., Chen Y., and Arai S. 2002. Helium in the Archean komatiites revisited: Significantly high ^{3}He/^{4}He ratios revealed by fractional crushing gas extraction. *Earth and Planetary Science Letters* 196:213–225.
Meshik A., Mabry J., Hohenberg C., Marrocchi Y., Pravdivtseva O., Burnett D., Olinger C., Wiens R., Reisenfeld D., Allton J., McNamara K., Stansbery E., and Jurewicz A. J. G. 2007. Constraints on neon and argon isotopic fractionation in solar wind. *Science* 318:433–435.
Miura Y. N., Hidaka H., Nishiizumi K., and Kusakabe M. 2007. Noble gas and oxygen isotope studies of aubrites: A clue to origin and histories. *Geochimica et Cosmochimica Acta* 71:251–270.
Moreira M. and Madureira P. 2005. Cosmogenic helium and neon in 11 Myr old ultramafic xenoliths: Consequences for mantle signatures in old samples. *Geochemistry Geophysics Geosystems* 6. https://doi.org/10.1029/2005GC000939.
Mortimer J., Verchovsky A. B., and Anand M. 2016. Predominantly non-solar origin of nitrogen in lunar soils. *Geochimica et Cosmochimica Acta* 193:36–53.
Murty S. V. S. and Mahajan R. R. 2004. Trapped noble gases and nitrogen components in Martian meteorites: Vacuum crushing and pyrolysis studies (abstract). *Meteoritics & Planetary Science* 39:5046. A75.
Nishiizumi K. 2004. Exposure histories of lunar and Martian meteorites (abstract). *Meteoritics & Planetary Science* 39:5108. A77.
Noble S. K., Keller L. P., and Pieters C. M. 2005. Evidence of space weathering in regolith breccias I: Lunar regolith breccias. *Meteoritics & Planetary Science* 40:397–408.
Noguchi T., Kimura M., Hashimoto T., Konno M., Nakamura T., Zolensky M. E., Okazaki R., Tanaka M.,

Tsuchiyama A., Nakato A., Ogami T., Ishida H., Sagae R., Tsujimoto S., Matsumoto T., Matsuno J., Fujimura A., Abe M., Yada T., Mukai T., Ueno M., Okada T., Shirai K., and Ishibashi Y. 2014. Space weathered rims found on the surfaces of the Itokawa dust particles. *Meteoritics & Planetary Science* 49:188–214.

Okazaki R., Nakamura T., Takaoka N., and Nagao K. 2003. Noble gases in ureilites released by crushing. *Meteoritics & Planetary Science* 48:767–781.

Okazaki R., Takaoka N., Nagao K., and Nakamura T. 2010. Noble gases in enstatite chondrites released by stepped crushing and heating. *Meteoritics & Planetary Science* 45:339–360.

Ott U. 2002. Noble gases in meteorites—Trapped components. In *Noble gases in geochemistry and cosmochemistry*, edited by Porcelli D., Ballentine C. J., and Wieler R. Reviews in Mineralogy and Geochemistry, vol. 47. Washington, D.C.: Mineralogical Society of America. pp. 71–100.

Ott U., Löhr H.-P., and Begemann F. 1996. Etching and crushing SNCs: More noble gas data (abstract). *Meteoritics & Planetary Science* 31:A103.

Owen T., Mahaffy P. R., Niemann H. B., Atreya S., and Wong M. 2001. Protosolar nitrogen. *The Astrophysical Journal* 553:L77–L79.

Ozima M., Miura Y. N., and Podosek F. A. 2004. Orphan radiogenic noble gases in lunar breccias: Evidence for planet pollution of the Sun? *Icarus* 170:17–23.

Palma R. L., Becker R. H., Pepin R. O., and Schlutter D. J. 2002. Irradiation records in regolith materials, II: Solar wind and solar energetic particle components in helium, neon, and argon extracted from single lunar mineral grains and from the Kapoeta howardite by stepwise pulse heating. *Geochimica et Cosmochimica Acta* 66:2929–2958.

Phakey P. P., Hutcheon I. D., Rajan R. S., and Price P. B. 1972. Radiation effects in soils from five lunar missions. Proceedings, 3rd Lunar Science Conference. pp. 2905–2915.

Raquin A. and Moreira M. 2009. Atmospheric $^{38}Ar/^{36}Ar$ in the mantle: Implications for the nature of the terrestrial parent bodies. *Earth and Planetary Science Letters* 287:551–558.

Reimer O., Menn W., Hof M., Simon M., Davis A. J., Labrador A. W., Mewaldt R. A., Schindler S. M., Barbier L. M., Christian E. R., Krombel K. E., Mitchell J. W., Ormes J. F., Streitmatter R. E., Golden R. L., Stochaj S. J., Webber W. R., and Rasmussen I. L. 1998. The cosmic-ray $^{3}He/^{4}He$ ratio from 200 MeV per nucleon^{-1} to 3.7 GeV per nucleon^{-1}. *The Astrophysical Journal* 496:490–502.

Renne P. R., Mundil R., Balco G., Min K., and Ludwig K. R. 2010. Joint determination of ^{40}K decay constants and $^{40}Ar^*/^{40}K$ for the Fish Canyon sanidine standard, and improved accuracy for $^{40}Ar/^{39}Ar$ geochronology. *Geochimica et Cosmochimica Acta* 74:5349–5367.

Renne P. R., Balco G., Ludwig K. R., Mundil R., and Min K. 2011. Response to the comment by W. H. Schwarz et al on "Joint determination of ^{40}K decay constants and $^{40}Ar^*/^{40}K$ for the Fish Canyon sanidine standard and improved accuracy for $^{40}Ar/^{39}Ar$ geochronology" by P. R. Renne et al (2010). *Geochimica et Cosmochimica Acta* 75:5097–5100.

Righter K. and Gruener J. 2013. The Lunar Meteorite Compendium. http://curator.jsc.nasa.gov/antmet/lmc/. Accessed June 4, 2015.

Scarsi P. 2000. Fractional extraction of helium by crushing of olivine and clinopyroxene phenocrysts: Effects on the $^{3}He/^{4}He$ measured ratio. *Geochimica et Cosmochimica Acta* 64:3751–3762.

Schaeffer G. A. and Schaeffer O. A. 1977. ^{40}Ar-^{39}Ar ages of lunar rocks. Proceedings, 8th Lunar Science Conference. pp. 2253–2300.

Schultz L. and Franke L. 2004. Helium, neon, and argon in meteorites: A data collection. *Meteoritics & Planetary Science* 39:1889–1890.

Schwarz W. H. and Trieloff M. 2007. Intercalibration of ^{40}Ar-^{39}Ar age standards NL25, HB3gr hornblende, GA-1550, SB-3, HD-B1 biotite and BMus/2 muscovite. *Chemical Geology* 242:218–231.

Schwarz W. H., Kossert K., Trieloff M., and Hopp J. 2011. Comment on the "Joint determination of ^{40}K decay constants and $^{40}Ar^*/^{40}K$ for the Fish Canyon sanidine standard and improved accuracy for $^{40}Ar/^{39}Ar$ geochronology" by Paul R. Renne et al (2010). *Geochimica et Cosmochimica Acta* 75:5094–5096.

Shuster D. L. and Cassata W. S. 2015. Paleotemperatures at the lunar surfaces from open system behaviour of cosmogenic ^{38}Ar and radiogenic ^{40}Ar. *Geochimica et Cosmochimica Acta* 155:154–171.

Sokol A. K., Fernandes V. A., Schulz T., Bischoff A., Burgess R., Clayton R. N., Münker C., Nishiizumi K., Palme H., Schultz L., Weckwerth G., Mezger K., and Horstmann M. 2008. Geochemistry, petrology and ages of the lunar meteorites Kalahari 008 and 009: New constraints on early lunar evolution. *Geochimica et Cosmochimica Acta* 72:4845–4873.

Steiger R. H. and Jäger E. 1977. Subcommission on Geochronology: Convention on the use of decay constants in geo- and cosmochronology. *Earth and Planetary Science Letters* 36:359–362.

Takaoka N. and Nakamura T. 1996. A possible site trapping noble gases in Happy Canyon enstatite chondrite: Microbubbles (abstract). 21st NIPR Symposium on Antarctic Meteorites. pp. 167–169.

Takaoka N., Okazaki R., Nakamura T., and Nagao K. 1998. Noble gases released from Yamato-74063 primitive achondrite by crushing (abstract). 23rd NIPR Symposium on Antarctic Meteorites. pp. 145–147.

Tera F., Papanastassiou D. A., and Wasserburg G. J. 1974. Isotopic evidence for a terminal lunar cataclysm. *Earth and Planetary Science Letters* 22:1–21.

Trieloff M. 1993. Datierung impaktmetamorpher Gesteine und methodische Ergänzungen zur ^{40}Ar-^{39}Ar Altersbestimmungstechnik. Ph.D. thesis. University of Heidelberg, Heidelberg, Germany.

Trieloff M., Reimold W. U., Kunz J., Boer R. H., and Jessberger E. K. 1994. ^{40}Ar-^{39}Ar thermochronology of pseudotachylite at the Ventersdorp Contact Reef, Witwatersrand Basin. *South African Journal of Geology* 97:365–384.

Trieloff M., Deutsch A., and Jessberger E. K. 1998. The age of the Kara impact structure, Russia. *Meteoritics & Planetary Science* 33:361–372.

Trieloff M., Falter M., and Jessberger E. K. 2003. The distribution of mantle and atmospheric argon in oceanic basalt glasses. *Geochimica et Cosmochimica Acta* 67:1229–1245.

Trieloff M., Korochantseva E. V., Buikin A. I., Hopp J., Ivanova M. A., and Korochantsev A. V. 2018. The

Chelyabinsk meteorite: Thermal history and variable shock effects recorded by the ^{40}Ar-^{39}Ar system. *Meteoritics & Planetary Science* 53:343–358. https://doi.org/10.1111/maps.13012.

Turner G. 1970. ^{40}Ar-^{39}Ar age determination of lunar rock 12013. *Earth and Planetary Science Letters* 9:177–180.

Turner G. 1971. ^{40}Ar-^{39}Ar dating: The optimization of irradiation parameters. *Earth and Planetary Science Letters* 10:227–234.

Turner G. 1977. Potassium-argon chronology of the Moon. *Physics and Chemistry of the Earth* 10:145–195.

Verchovsky A. B., Fisenko A. V., Semjonova L. F., and Pillinger C. T. 1997. Heterogeneous distribution of xenon-HL within presolar diamonds. *Meteoritics & Planetary Science* 32:A131–A132.

Verchovsky A. B., Fisenko A. V., Semjonova L. F., Wright I. P., Lee M. R., and Pillinger C. T. 1998. C, N, and noble gas isotopes in grain size separates of presolar diamonds from Efremovka. *Science* 281:1165–1168.

Verchovsky A. B., Sephton M. A., Wright I. P., and Pillinger C. T. 2002. Separation of planetary noble gas carrier from bulk carbon in enstatite chondrites during stepped combustion. *Earth and Planetary Science Letters* 199:243–255.

Verchovsky A. B., Mortimer J., Buikin A. I., and Anand M. 2017. Trapping of atmospheric gases during crushing of lunar samples (abstract #2204). 48th Lunar and Planetary Science Conference. CD-ROM.

Wieler R. 2002. Noble gases in the solar system. In *Noble gases in geochemistry and cosmochemistry*, edited by Porcelli D., Ballentine C. J., and Wieler R. Reviews in Mineralogy and Geochemistry, vol. 47. Washington, D.C.: Mineralogical Society of America. pp. 21–70.

Wieler R. 2016. Do lunar and meteoritic archives record temporal variations in the composition of solar wind noble gases and nitrogen? A reassessment in the light of Genesis data. *Chemie der Erde* 76:463–480.

Wieler R. and Heber V. S. 2003. Noble gas isotopes on the Moon. *Space Science Reviews* 106:197–210.

Wieler R., Baur H., and Signer P. 1986. Noble gases from solar energetic particles revealed by closed system stepwise etching of lunar soil minerals. *Geochimica et Cosmochimica Acta* 50:1997–2017.

Wiens R. C. 1988. Noble gases released by vaccum crushing of EETA79001 glass. *Earth and Planetary Science Letters* 91:55–65.

Yaniv A. and Heymann D. 1972. Atmospheric ^{40}Ar in lunar fines. Proceedings, 3rd Lunar Science Conference. pp. 1967–1980.

Yokochi R., Marty B., Pik R., and Burnard P. 2005. High ^{3}He/^{4}He ratios in peridotite xenoliths from SW Japan revisited: Evidence for cosmogenic ^{3}He released by vacuum crushing. *Geochemistry Geophysics Geosystems* 6. https://doi.org/10.1029/2004GC000836.